gene encoding the cholesterol side-chain cleavage enzyme, an essential enzyme for steroidogenesis) was integrated into the MSCs, and GFP-positive MSCs were then separated by fluorocytometry. Finally, to achieve the efficient differentiation of the isolated MSCs *in vitro*, the orphan nuclear receptor, steroidogenic factor (SF)-1 was ectopically expressed in MSCs. MSCs successfully differentiated into steroidogenic cells using any of these procedures. These results indicate that MSCs represent a useful source of stem cells for producing steroidogenic cells that may provide basis for their use in cell and gene therapy.

## Materials and Methods

### *Animals*

GFP transgenic rats [SD TgN(act-EGFP)OsbCZ-004] were kindly provided by Dr. M. Okabe (Osaka University, Osaka, Japan). Sprague Dawley rats were purchased from Sankyo (Shizuoka, Japan). At all times, the animals were treated according to National Institutes of Health guidelines. The donor animals used in this study were generally 4–5 wk old, and the recipient animals were 3 wk old.

### *Histology and immunofluorescence analysis*

Immunohisto- and cytochemical staining with antirat P450 side-chain cleaving enzyme (P450scc) (C-16; Santa Cruz Biotechnology, Santa Cruz, CA), antimouse 3β-hydroxysteroid dehydrogenase I (3β-HSD I) (kindly provided by Dr. A. Payne, Stanford University Medical Center, Stanford, CA), antipig cytochrome P450 17 α-hydroxylase (P450c17) (kindly provide by Dr. D. Hales, University of Illinois at Chicago, Chicago, IL) or anti-GFP (Medical & Biological Laboratories Co., Ltd.) were performed on 10-μm frozen sections or cultured cells on glass slides using standard protocols. Appropriate Cy3- or fluorescein isothiocyanate-conjugated secondary antibodies (Sigma, St. Louis, MO) were used for detection.

### *Cell culture, stable transfection, and hormone assay*

MSCs from GFP transgenic rats were collected and cultured as described by Pochampally *et al.* (14). Mouse (KUM9) (15) or human (hMSC-hTERT-E6/E7) (16) bone marrow-derived MSCs were maintained in Iscova's MEM or DMEM with 10% fetal calf serum. Plasmid DNA was transfected using the LipofectAmine PLUS reagent (Invitrogen, Carlsbad, CA) or calcium phosphate coprecipitation. Cells were used for the experiments after 10–12 passages, and steroid hormone production was sustained for at least 4 months. The levels of each steroid hormone in the media were measured by RIA.

### *Transplantation*

Bone marrow cells from TgN(ActbEGFP) transgenic rats ($1 \times 10^6$) were injected into the testes of 3-wk-old SD rats. Two to three weeks after transplantation, testes were removed to examine histochemically survival and differentiation of transplanted cells.

### *Plasmid construction*

A 2.3-kb fragment of the human CYP11A (P450scc gene) promoter that functions specifically in steroidogenic organs (17) was obtained by PCR using pSCC2300-LacZ (kindly provided by Dr. B. C. Chung, Institute of Molecular Biology, Taipei, Taiwan) as a template and integrated into a promoter-less pEGFP-1 vector (CLONTECH, Palo Alto, CA). The *Eco*RI-*Stu*I restriction fragment, containing the CYP11A promoter-GFP, was then excised and inserted into *Eco*RI and *Swa*I site of pPUR (CLONTECH). The expression vector for rat SF-1 cDNA containing the entire coding region was generated by RT-PCR and subcloned into pIRES-puro2 vector (CLONTECH).

### *FACS analysis and cell purification*

Cells were harvested by treatment with 0.25% trypsin/EDTA, after which they were neutralized with DMEM with 10% fetal calf serum, washed twice with PBS, and filtered through a 35-mm pore size nylon screen. FACS analysis was performed on a flow cytometer with a 488-nm argon laser and GFP-positive cells were isolated.

### *RT-PCR and real-time PCR*

Total RNA from the cultured cells was extracted using the Trizol reagent (Invitrogen). RT-PCR was performed as described previously (18). The reaction mixture was subjected to electrophoresis in a 1.5% agarose gel, and the resulting bands were visualized by staining with ethidium bromide. Real-time PCR was performed as described by Rutledge and Cote (19). Reagents for real-time PCR were purchased from Applied Biosystems (Warrington, UK), except for SYBER green PCR master mix (QIAGEN, Valencia, CA). Reactions were carried out and fluorescence was detected on a GeneAmp 7700 system (Applied Biosystems). The primers used are shown in Table 1.

### *Western blot analysis*

The extraction of protein from the cultured cells and subsequent quantification was performed as described previously (20). Equal amounts of protein (50 μg) were resolved by 12.5% SDS-PAGE and transferred to polyvinylidene difluoride membranes. Western blot analyses of SF-1, steroidogenic acute regulatory protein (StAR), P450scc, 3β-HSD I, P450c17, and β-tubulin were carried out with antisera directed against SF-1 (Ad4BP, kindly provided by Dr. K. Morohashi, National Institute of Basic Biology, Okazaki, Japan), StAR (kindly provided by Dr. W. Miller, University of California, San Francisco, CA) (21), P450scc (kindly provided by Dr. B. C. Chung) (22), 3β-HSD I (kindly provided by Dr. A. Payne), P450c17 (kindly provided by Dr. D. Hales) (23), and β-tubulin (D-10, Santa Cruz). ECL Western blot reagents (Amersham Pharmacia Biotech, Piscataway, NJ) were used for detection.

## Results

### *Transplantation of rat bone marrow mesenchymal stem cells*

In the prepubertal testis, fetal-type Leydig cells are replaced by adult-type Leydig cells, which originate from mesenchymal precursor cells that are present in the testicular interstitium (12). To determine whether MSCs can be engrafted into the testis and converted into steroidogenic cells we took $1 \times 10^6$ bone marrow cells from TgN(ActbEGFP) transgenic rats that had been maintained in culture (Fig. 1A) and injected them into the testes of 3-wk-old SD rats. As shown in Fig. 1C, donor engraftment was confirmed (100%) at various periods after transplantation (1–4 wk). A histochemical examination revealed that the GFP-positive cells present in the testes were located in the interstitium and were not observed within the seminiferous tubules (Fig. 1D). An immunohistochemical study showed that most of the GFP-positive cells in the interstitium were also positive for three Leydig cell markers, P450scc (Fig. 1E), 3β-HSD I, and P450c17 (data not shown). These results indicate that donor derived-plastic adhered marrow cells had in fact differentiated into steroidogenic Leydig-like cells *in vivo*.

### *Gene promoter sorting*

Although these data suggest that the injected stem cells differentiated into Leydig cells, the apparent stem cell plasticity may also be explained by possible cell-nuclear fusion between donor and recipient cells, as has been recently suggested (24). Therefore, we next performed *in vitro* experiments to determine whether purified murine MSCs (mMSCs), KUM9 (15), have the capacity to differentiate into steroidogenic cells. To detect a cell population committed to

**TABLE 1.** Primers for RT-PCR and real-time PCR

| Gene | Sequence | Gene | Sequence |
|---|---|---|---|
| RT-PCR | | RT-PCR | |
| SF-1 | F-CGCACAGTCCAGAACAACAAGCA<br>R-CGGTTAGAGAAGGCAGGATAGAG | hHSD3b2 | F-CAGTGTGCCAGTCTTCATCT<br>R-AGCAGGAAGCCAATCCAGTA |
| mStAR | F-GAAGGAAAGCCAGCAGGAGAACG<br>R-CTCTGATGACACCACTCTGCTCC | hP450c17 | F-CATGCTGGACACACTGATGC<br>R-GGTTGTATCTCTAAAATCTGT |
| mP450scc | F-TTCCGCTTTTCCTTTGAGTCCAT<br>R-GTGTCTCCTTGATGCTGGCTTTC | hHSD17b3 | F-GCAGATTTTACAAAAGATGACAT<br>R-TCATGGGCAAGGCAGCCACAGGT |
| mHSD3b1 | F-ACTGCAGGAGGTCAGAGCT<br>R-GCCAGTAACACAGAATACC | hP450c21 | F-TGCCTGCCTATTACAAATGT<br>R-GGTGAAGCAAAAAAACCACG |
| mHSD3b6 | F-TCTGGAGGAGATCAGGGTC<br>R-GCCCGTACAACCGAGAATATT | hP45011 b1 | F-ACATTGGTGCGCGTGTTCCTC<br>R-GAGACGTGATTAGTTGATGGC |
| mP450c17 | F-AAATAATAACACTGGGGAAGGC<br>R-TGGGTGTGGGTGTAATGAGATGG | hP450 11b2 | F-TACAGGTTTTCCTCTACTCG<br>R-AGATGCAAGACTAGTTAATC |
| mP450c21 | F-AGAGGATCCGCTTGGGGCTGC<br>R-GGAGGAATTCCTTATGGATGGC | hP450aro | F-CTGGAAGAATGTATGGACTT<br>R-GATCATTTCCAGCATGTTTT |
| mP450 11b1 | F-TCACCAAATGTATCAAGAATGTGT<br>R-CCATCTGCACATCCTCTTTCTCTT | β-Actin | F-GGGAAATCGTGCGTGACATTAAG<br>R-TGTGTTGGCGTACAGGTCTTTG |
| mP450 11b2 | F-CCAACAGATGTATCTGGAAGGTGC<br>R-CCATCTGCACATCCTCTTGCCTCA | hIGF-2 | F-AGTCGATGCTGGTGCTTCTACCTCTT<br>R-TGCGGCAGTTTTGCTCACTTCCGATT |
| mLHR | F-CTCCACCTATCTCCCTGTC<br>R-TCTTTCTTCGGCAAATTCCTG | Real-time PCR | |
| mACTHR | F-GCTCCAAGGATCATTTACTTGC<br>R-CGCCAGGAGGCTTAACATAAC | mP450scc | F-CCAGTGTCCCCATGCTCAAC<br>R-TGCATGGTCCTTCCAGGTCT |
| GAPDH | F-ACCACAGTCCATGCCATCAC<br>R-TCCACCACCCTGTTGCTGA | mHSD3b1 | F-TAACAATTTAACAGCCCCTCCTAAGG<br>R-ATCCAGCCATGGTCAACACA |
| GFP | F-TGACCACCCTGACCTACGGCGT<br>R-GGTAGTGGTTGTCGGGCAGCA | mHSD3b6 | F-AAACCATCCTCCACTGTTCTAGCT<br>R-TGGAGATGGTCAGCCACAAG |
| mHSD17b3 | F-ATTTTACCAGACAAGACATCT<br>R-GGGGTCAGCACCTGAATAATG | mP450c17 | F-AGTTTGCCATCCCGAAGGA<br>R-CTGGCTGGTCCATTCATTT |
| mP450aro | F-TCAATACCAGGTCCTGGCTA<br>R-GTATGCACTGATTCACGTTC | mHSD17b3 | F-TGGGACAATGGGCAGTGAT<br>R-GCCAACTCAAATGAATAGGCTTTC |
| hStAR | F-GAGAGTCAGCAGGACAATGG<br>R-CTGGTTGATGATGCTCTTGG | β-Actin | F-CAACCGTGAAAAGATGACCCAGATC<br>R-AGTCCATCACAATGCCTGTGGTAC |
| hP450scc | F-TAGTGTCTCCTTGATGCTGG<br>R-GAAAGGAAGTGTTCACCACG | | |

F, Forward; R, reverse.

the steroidogenic lineage, we first introduced a human CYP11A1 promoter/GFP gene construct into the mMSCs. This was accomplished by using a 2.3-kb fragment of the promoter region of the human CYP11A1 (a gene that encodes cytochrome P450scc, cholesterol side-chain cleavage enzyme), which has been shown to selectively drive transgene expression to adrenal and gonadal steroidogenic cells (17). In some of the transformed cell lines, GFP fluorescence was detected, as shown in Fig. 2, B and C, but the number of GFP-expressing cells was very low. Thus, GFP-positive cells were enriched by sorting with flow cytometry (Fig. 2E, 1–5% of total cells). As shown in Fig. 2, F and G, enriched GFP-positive cells were also positive for P450scc, indicating that a very small but distinct portion of the mMSCs had spontaneously differentiated into cells that produce the steroid hormone-synthesizing enzyme. Further analysis of the differentiated cells revealed the expression of several genes that are specific to testicular Leydig cells, as shown in Fig. 2H. These include a nuclear orphan receptor SF-1, 3β-HSD types I and VI, and LH receptor (Fig. 2H, lane SCC+). LH receptor and 3β-HSD VI are known to be typical markers for androgen producing cells, such as Leydig cells (25). These observations further support the *in vivo* findings that rodent MSCs have the capacity to differentiate into Leydig-like cells in the testis.

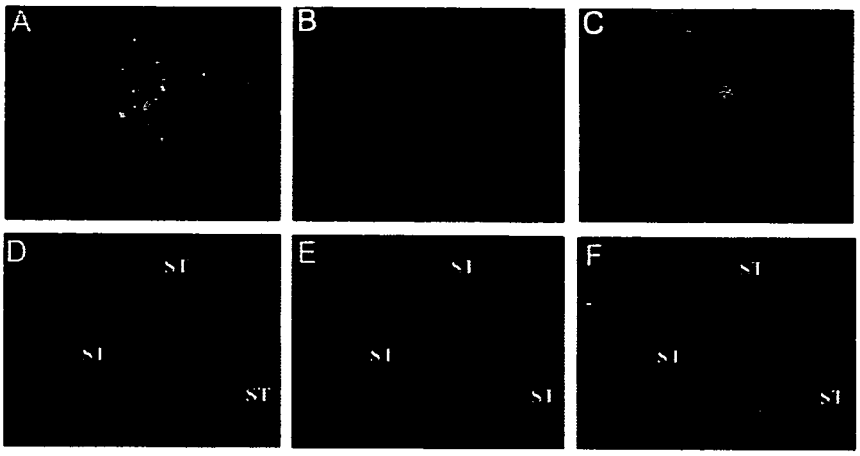


FIG. 1. Transplantation of GFP-positive MSCs into the testis. A, Fluorescence view of MSCs from a green rat 3 d after the first passage. Fluorescence microscopic view of testis before (B) or 3 wk after (C) MSC transplantation. Double staining of frozen sections from the testis 5 wk after MSC transplantation with anti-GFP (D) and anti-P450scc (E) antibodies. F, Merged fluorescent image of D and E. ST, Seminiferous tubule.

*Stable transfection of SF-1 into mouse MSCs*

It is noteworthy that SF-1 expression was induced in the GFP-positive cells (Fig. 2H). SF-1, also known as Ad4BP, regulates the cell-specific expression of a variety of proteins that are involved in steroidogenesis, in addition to its roles in reproduction and gonadal differentiation (26). Therefore, we next examined the effects of the stable transfection of SF-1 to mMSCs. Various cell lines that stably express SF-1 were isolated. As shown in Fig. 3C, SF-1-induced morphological changes in the cells, such as the accumulation of numerous lipid droplets. However, the transformed cells did not express steroidogenic enzyme genes or produce any steroid

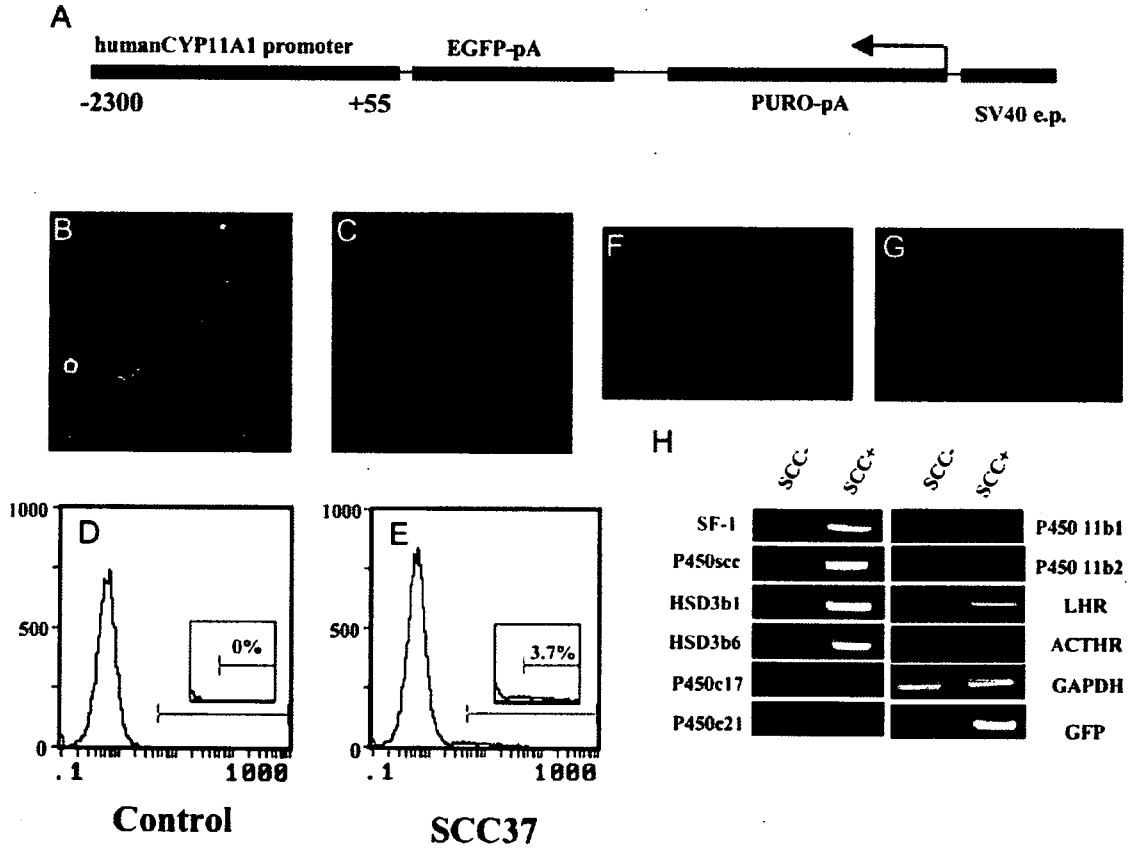


FIG. 2. Spontaneous differentiation of KUM9 into steroidogenic cells. A, Schematic representation of the SCC-reporter gene (SCC-GFP). The SCC-GFP reporter plasmid contains the 2300-bp upstream sequence of the human CYP11A1 gene and the puromycin-*N*-acetyltransferase gene (PURO-pA) driven by the Simian virus 40 early promoter (SV40 e.p.). Phase-contrast (B) and fluorescent (C) images of mMSCs transfected with SCC-GFP and selected by puromycin are shown. Flow cytometric analysis of enhanced GFP (EGFP) expression in KUM9 transfected with control-GFP (D) or SCC-GFP (E) are shown. KUM9-derived cells expressing GFP (F) under the control of the human CYP11A1 promoter were immunocytochemically stained with anti-P450scc antibody (G). H, SCC-GFP-positive (SCC+) and negative (SCC−) populations were sorted and analyzed for various marker genes by RT-PCR.

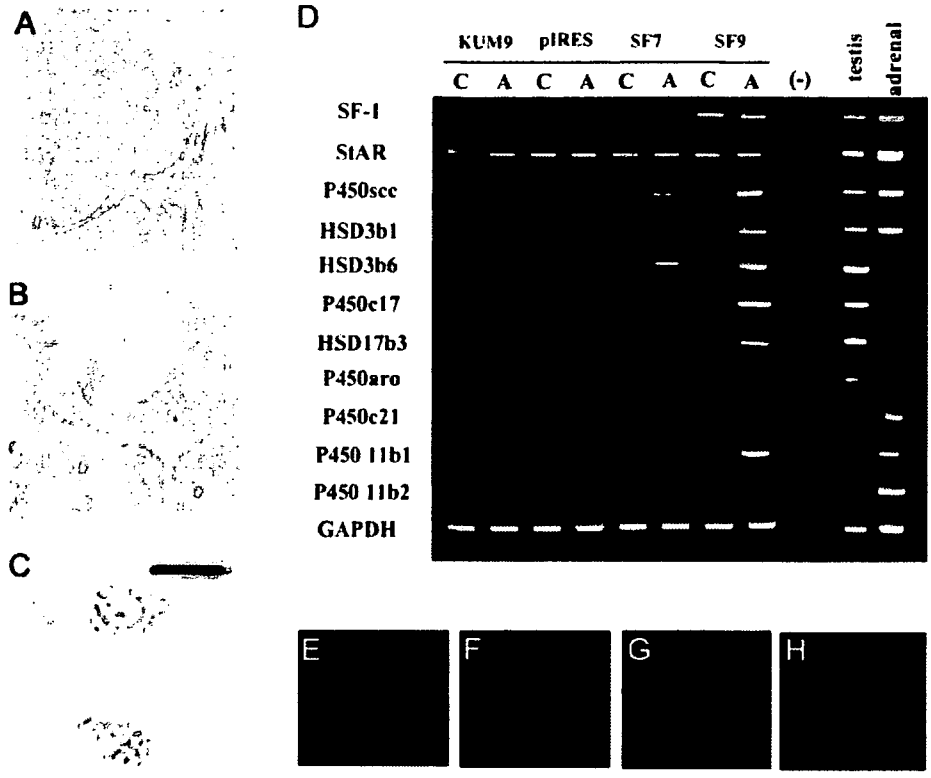


FIG. 3. Differentiation of KUM9 into steroidogenic cells. Phase-contrast images of mMSCs untransfected (A) or stably transfected with the control (B) or the SF-1-expression (C) vectors are shown. An immunoblot analysis was performed with an antibody against SF-1 (*insets*). D, RT-PCR analysis of each clones cultured with or without 8-bromoadenosine-cAMP (8br-cAMP) for 7 d (C: without 8br-cAMP; A: with 8br-cAMP). Data were compared with those from mouse adrenal and testicular tissues. Fluorescent images of 4′,6′-diamino-2-phenylindole staining (E and G) and a P450scc immunostaining (F and H) of KUM9 transfected with the SF-1-expressing vector and then cultured with (G and H) or without 8br-cAMP (E and F).

hormones (Fig. 3D and Table 2). Therefore, we next added cAMP to the cultures because cAMP is known to induce steroidogenesis in a number of steroidogenic cell lines. Treatment of confluent cultures with cAMP was found to induce both P450scc mRNA (Fig. 3D) and protein (Fig. 3H) in the transformed cell lines, SF7 and SF9, whereas no induction was observed in untransfected (KUM9) or vector-transfected (pIRES) mMSCs (Fig. 3D). Treatment of the cells for a period of 7 d further induced the expression of other steroidogenic enzyme genes, as shown in Fig. 3D. Several cell lines showed similar expression patterns (two of which are shown in Fig. 3D).

3β-HSD types I and VI were induced 3 d after cAMP treatment (Fig. 4). In the testis, the formation of testosterone is dependent on 3β-HSD activity, and isoform types I and VI have been shown to be expressed in the adult mouse testis (27). P450c17 and 17β-hydroxysteroid dehydrogenase III (17β-HSD III) were induced 5 d after the treatment (Fig. 4). It is interesting to note that the order of induction of the enzymes is similar to the sequential order for the steroid hormone synthetic pathway. 3β-HSD enzymes are essential for the production of progesterone, and P450c17 and 17β-HSD III are both required for the production of testosterone in testicular Leydig cells. Consistent with the expression pattern of the steroidogenic enzymes, testosterone was the major sex steroid hormone produced in the transformed cell line, SF9, when treated with cAMP for 7 d (Table 2). Two adrenal-specific steroid hormones, glucocorticoids and mineralocorticoids, were not detected in these cells. These results clearly demonstrate that the stable expression of SF-1 and the addition of cAMP induced the differentiation of mMSCs into steroidogenic cells and that these cells have properties that are similar to those of testicular Leydig cells.

**TABLE 2.** Production of steroid hormones by MSCs stably expressing SF-1 (SF9-KUM9 or SF4-hMSC) in the presence (+) or absence (−) of 8br-cAMP (ng/ml)

| Cell (cAMP) | Progesterone | Testosterone | Estradiol | Glucocorticoid | Aldosterone |
|---|---|---|---|---|---|
| pIRES-KUM9 (−) | N.D. | N.D. | N.D. | N.D. | N.D. |
| pIRES-KUM9 (+) | N.D. | N.D. | N.D. | N.D. | N.D. |
| SF9-KUM9 (−) | N.D. | N.D. | N.D. | N.D. | N.D. |
| SF9-KUM9 (+) | 24.3 ± 4.25 | 1.6 ± 0.29 | N.D. | N.D. | N.D. |
| pIRES-hMSC (−) | N.D. | N.D. | N.D. | N.D. | N.D. |
| pIRES-hMSC (+) | N.D. | N.D. | N.D. | N.D. | N.D. |
| SF4-hMSC (−) | N.D. | N.D. | N.D. | N.D. | N.D. |
| SF4-hMSC (+) | 270 ± 82.5 | 17.5 ± 0.20 | 0.21 ± 0.11 | 520 ± 200 | 1.56 ± 0.42 |

Data are means and SEM values of at least duplicate assays. N.D., No detectable values.

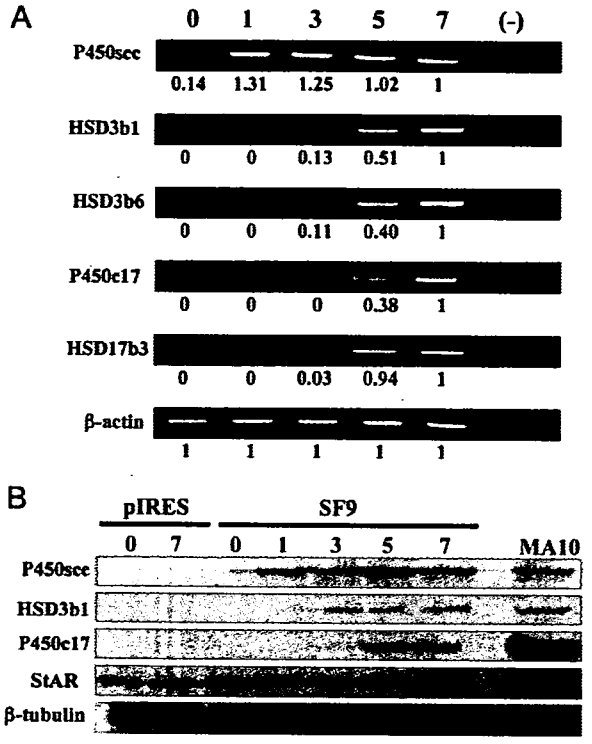


FIG. 4. Time-dependent induction of steroidogenic enzymes by cAMP. KUM9 cells stably transfected with SF-1-expression (SF9) or control (pIRES) vector were cultured and treated with 8-bromoadenosine-cAMP for the indicated times. A, P450scc, 3β-HSD I, 3β-HSD VI, P450c17, and 17β-HSD III mRNA levels were analyzed by RT-PCR and real-time PCR. Real-time PCR data are the mean values of at least triplicate assays. The 7-d value was arbitrarily taken as 1.0. B, Immunoblot analyses were performed with antibodies against StAR, P450scc, 3β-HSD I, P450c17, and β-tubulin using the same lysates. The data were compared with that from MA-10 cells treated with cAMP (4 h).

*Stable transfection of SF-1 into human MSCs*

We next examined the issue of whether the same approach could also be used to induce the differentiation of human MSCs (hMSCs) into steroidogenic cells. Similar to the results obtained with mMSCs, hMSCs (hMSC-TERT-E6/E7) expressed no steroidogenic enzymes or StAR before transfection with SF-1 even after cAMP treatment (Fig. 5). After SF-1 transfection, all the transformed cell lines became positive for StAR gene expression, and the expression levels were further increased by cAMP treatment. Most of the steroidogenic enzymes, P450scc, 3β-HSD II, P450c17, cytochrome P450 steroid 21-hydroxylase (P450c21), cytochrome P450 aromatase (P450arom), and cytochrome P450 steroid 11 β-hydroxylase, were also substantially induced by cAMP stimulation. A significant difference between mMSCs and hMSCs was the strong expression of the P450c21 gene in the case of hMSCs. This caused a difference in the kinds of steroids produced by mMSCs and hMSCs. As listed in Table 2, glucocorticoids were the major steroids produced by the transformed hMSCs, hSF4, whereas testosterone was the major product from the transformed mMSCs, mSF9. The hSF4 cells mainly produced cortisol, the major glucocorticoid produced by the human adrenal gland. These results clearly demonstrate that the stable expression of SF-1 and subsequent cAMP treatment induced the differentiation of hMSCs into steroidogenic cells. In addition, the cortisol-producing cells also expressed ACTH receptors and can respond to ACTH for the quick production of cortisol at nanomolar levels (data not shown).

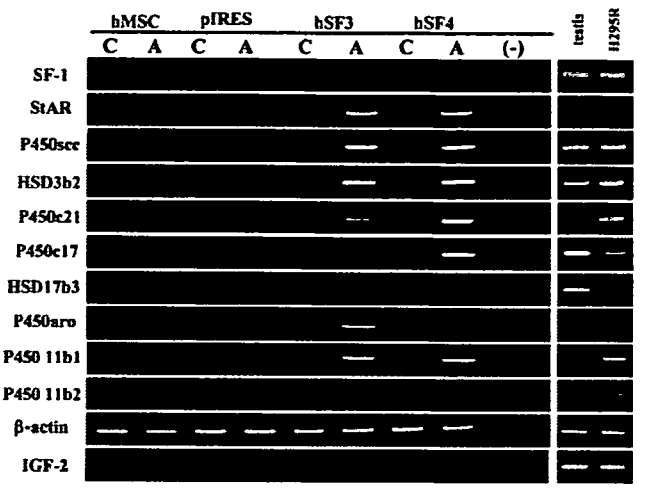


FIG. 5. Induction of steroidogenic enzymes in hMSCs. hMSCs were stably transfected with the control (pIRES) or SF-1-expression (SF3, -4) vector. RT-PCR analysis of each clone was cultured with or without 8-bromoadenosine-cAMP (8br-cAMP) for 7 d (C: without 8br-cAMP; A: with 8br-cAMP). The data were compared with that from human testis and NCI-H295R, a human adrenocortical tumor cell line, treated with cAMP (24 h).

Human MSCs also expressed P450arom as in the case of the human adrenocortical carcinoma NCI-H295R cell line (Fig. 5), whereas normal adrenal cells do not express it (28). However, hSF3 or -4 did not express IGF-II, an adrenocortical tumor marker. It has recently been shown that P450arom is expressed in human bone marrow stroma cells under certain conditions (29). Thus, it is probable that the expression of P450arom in hMSCs was not the result of a malignant phenotype or the differentiation of the cells by SF-1 and cAMP treatment.

*Stable transfection of SF-1 into cells other than MSCs*

We next examined the effects of transfection of SF-1 into several cell lines other than MSCs, *i.e.* a human cell line HEK293, murine embryonic stem cells, and murine cell lines F9 and NIH3T3. None of the transfected cell lines autonomously produced steroid hormones, although some were induced to express the P450scc and 3β-HSD genes (Fig. 6).

## Discussion

The findings presented herein demonstrate that rodent MSCs have the potential to differentiate into steroidogenic cells with characteristics that are very similar to testicular Leydig cells. It has been postulated that mesenchymal progenitors of Leydig cells are present in the testicular interstitium (12). Immature Leydig cells are gradually replaced by mature Leydig cells that are thought to differentiate from these mesenchymal progenitors during the prepubertal period. In fact, the injection of MSCs into the testis during this critical period caused the differentiation of MSCs into steroidogenic cells that were indistinguishable from Leydig cells. Concerning the *in vivo* experiments, the possibility of

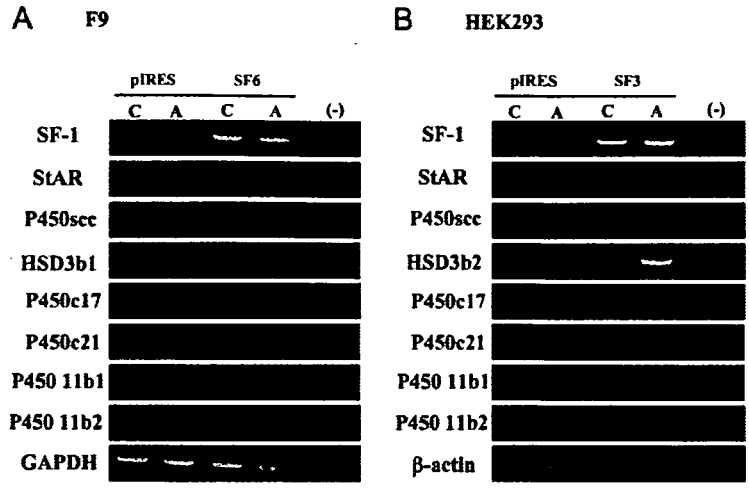


FIG. 6. Stable transfection of SF-1 and cAMP treatment for F9 (A) and HEK293 cells (B). RT-PCR analysis of steroidogenesis-related genes in each stable cell line transfected with SF-1 or pIRES (control) cultured with or without 8-bromoadenosine-cAMP (8br-cAMP) for 7 d (C: without 8br-cAMP; A: with 8br-cAMP).

cell fusion between donor MSCs and recipient testicular Leydig cells or their progenitor cells cannot be excluded. However, it should be emphasized that very small but distinct portions of mMSCs underwent spontaneous differentiation into Leydig-like cells *in vitro*. Lo *et al.* (30) demonstrated, by means of a cell transplantation assay, the presence of stem cells or progenitors for Leydig cells. Therefore, our data strongly suggest that bone marrow-derived MSCs share common properties with testicular MSCs or Leydig cell progenitors. Conversely, testicular MSCs or Leydig cell progenitors might also have pluripotent characteristics, similar to bone marrow-derived MSCs, as has been reported for some other MSCs (4, 31).

In addition, transfection of cultured mMSCs with SF-1 followed by cAMP stimulation resulted in their differentiation into Leydig cells. The same procedure also led to the successful induction of hMSCs into steroidogenic cells. In this case, however, most of the cell lines expressing SF-1 largely produced glucocorticoids rather than testosterone. This was mainly due to the strong induction of P450c21 gene expression in the hMSCs. To investigate the issue of whether hMSCs are able to differentiate into Leydig cells, we also injected hMSCs to the testis of nude mice or rats (data not shown). Unfortunately, the human cells did not survive for more than several weeks in the rodent testis.

Because the established cell lines need much longer times than general steroidogenic cells to produce steroid hormones by cAMP stimulation in this study, we speculate that cAMP treatment of this study is necessary for the induction of the cellular differentiation rather than direct stimulation of gene transcription of steroidogenic enzymes.

In hMSCs, the stable expression of SF-1 and cAMP treatment induced the expression of the StAR gene, which is essential for the transfer of cholesterol from the outer to the inner membrane of mitochondria in which the conversion of cholesterol to steroid hormones begins (21). The same treatment failed to induce StAR gene expression in several cell lines (other than MSCs) including embryonic stem (ES) cells and therefore failed to induce any steroid hormones. The expression of the P450scc or 3β-HSD gene was induced at low levels in some of them, however (Fig. 6). It has been reported that the stable transfection of SF-1 into ES cells results in morphological changes and the induction of P450scc enzyme expression, (32). No autonomous production of steroid hormones was observed, however, probably because of the deficiency of cholesterol storage and mobilization and the lack of StAR protein expression (32). Therefore, our present observations suggest that MSCs, but not ES cells, are excellent precursors of steroidogenic cells. In contrast to human cells, StAR was constitutively expressed in KUM9 as well as the freshly isolated rat MSCs (our unpublished data). Therefore, we speculate that StAR gene expression is not always under the control of SF-1, and the pattern of expression may be different between species, even in the same tissues. In addition to the steroidogenesis, the movement of cholesterol to the inner mitochondrial membrane is also important for its metabolism, because one of the rate-determining steps, the 27-hydroxylation of cholesterol, is catalyzed by sterol 27-hydroxylase, which is located in the inner mitochondrial membrane (33, 34). Cholesterol metabolites, such as oxysterols have been proposed to be potential regulators of genes in cholesterol homeostasis (33). We found that sterol 27-hydroxylase mRNA was detectable in rat and mouse MSCs (data not shown), suggesting that it is involved in cholesterol metabolism. Therefore, it is assumed that the StAR protein in KUM9 is present to promote the cholesterol metabolism, despite the fact that steroidogenesis does not take place. In support of this hypothesis, ectopic expression of the StAR protein increases the metabolism of cholesterol in rat primary hepatocytes (34).

Gondo *et al.* (35) recently reported that the adenovirus-mediated forced expression of SF-1 transforms primary long-term cultured murine bone marrow cells into ACTH-responsive steroidogenic cells. In contrast to our observation obtained from murine MSCs, their steroidogenic cells produce both gonadal and adrenal steroids. There are two possible explanations for their results: 1) their cells were a mixed adrenal/gonadal phenotype or 2) were a mixture of adrenal or gonadal phenotypic cells. The latter seems to be more likely because our study clearly demonstrated the differentiation of adult stem cells derived from both murine and human into gonadal or adrenal steroidogenic cells. Therefore, with respect to the difference between mouse and human cells, we assume that the mouse MSCs used in our study were already committed to the gonadal lineage, whereas the hMSCs were already committed to

the adrenal lineage. In support of this hypothesis, it has frequently been reported that MSCs are heterogeneous populations that have a different differentiation potential (1, 2, 10). In a future study, the same treatment of various mouse or human MSCs need to be carried out, followed by observations of whether both adrenal and gonadal phenotypes are obtained. This might also provide a tool for revealing the pathway leading to the differentiation of the cells into adrenal or gonadal steroidogenic cells.

In summary, we demonstrate here that MSCs have the capacity to differentiate into steroidogenic cells, both *in vivo* and *in vitro*. MSCs represent not only a powerful tool for studies of the differentiation of the steroidogenic lineage but may also offer a possible clinical stem cell resource for diseases of steroidogenic organs.

## Acknowledgments

We are grateful to Drs. K. Morohashi, W. Miller, B. C. Chung, A. Payne, and D. Hales for providing plasmids and antisera. We also thank Drs. M. Ascoli and J. Toguchida for the generous gifts of MA10 and hMSCs and Ms. Y. Inoue, T. Satake, and K. Matsuura for technical assistance.

Received February 8, 2006. Accepted May 16, 2006.

Address all correspondence and requests for reprints to: Kaoru Miyamoto, Department of Biochemistry, Faculty of Medical Sciences, University of Fukui, Shimoaizuki, Matsuoka-cho, Fukui 910-1193, Japan. E-mail: kmiyamot@fmsrsa.fukui-med.ac.jp.

This work was supported in part by a grant from the Smoking Research Foundation and the 21st Century Center of Excellence Program (Medical Science).

All authors (T.Y., T.M., K.Y., H.K., T.S., M.Y., T.K., Z.S., A.U., K.M.) have nothing to declare.

## References

1. **Friedenstein AJ, Gorskaja JF, Kulagina NN** 1976 Fibroblast precursors in normal and irradiated mouse hematopoietic organs. Exp Hematol 4:267–274
2. **Prockop DJ** 1997 Marrow stromal cells as stem cells for nonhematopoietic tissues. Science 276:71–74
3. **Ferrari G, Cusella-De Angelis G, Coletta M, Paolucci E, Stornaiuolo A, Cossu G, Mavilio F** 1998 Muscle regeneration by bone marrow-derived myogenic progenitors. Science 279:1528–1530
4. **Lee OK, Kuo TK, Chen WM, Lee KD, Hsieh SL, Chen TH** 2004 Isolation of multipotent mesenchymal stem cells from umbilical cord blood. Blood 103: 1669–1675
5. **D'Amour KA, Gage FH** 2003 Genetic and functional differences between multipotent neural and pluripotent embryonic stem cells. Proc Natl Acad Sci USA 100(Suppl 1):11866–11872
6. **De Ugarte DA, Morizono K, Elbarbary A, Alfonso Z, Zuk PA, Zhu M, Dragoo JL, Ashjian P, Thomas B, Benhaim P, Chen I, Fraser J, Hedrick MH** 2003 Comparison of multi-lineage cells from human adipose tissue and bone marrow. Cells Tissues Organs 174:101–109
7. **Kopen GC, Prockop DJ, Phinney DG** 1999 Marrow stromal cells migrate throughout forebrain and cerebellum, and they differentiate into astrocytes after injection into neonatal mouse brains. Proc Natl Acad Sci USA 96:10711–10716
8. **Ortiz LA, Gambelli F, McBride C, Gaupp D, Baddoo M, Kaminski N, Phinney DG** 2003 Mesenchymal stem cell engraftment in lung is enhanced in response to bleomycin exposure and ameliorates its fibrotic effects. Proc Natl Acad Sci USA 100:8407–8411
9. **Chamberlain JR, Schwarze U, Wang PR, Hirata RK, Hankenson KD, Pace JM, Underwood RA, Song KM, Sussman M, Byers PH, Russell DW** 2004 Gene targeting in stem cells from individuals with osteogenesis imperfecta. Science 303:1198–1201
10. **Prockop DJ, Gregory CA, Spees JL** 2003 One strategy for cell and gene therapy: harnessing the power of adult stem cells to repair tissues. Proc Natl Acad Sci USA 100(Suppl 1):11917–11923
11. **Hatano O, Takakusu A, Nomura M, Morohashi K** 1996 Identical origin of adrenal cortex and gonad revealed by expression profiles of Ad4BP/SF-1. Genes Cells 1:663–671
12. **Roosen-Runge EC, Anderson D** 1959 The development of the interstitial cells in the testis of the albino rat. Acta Anat (Basel) 37:125–137
13. **Holmes PV, Dickson AD** 1971 X-zone degeneration in the adrenal glands of adult and immature female mice. J Anat 108:159–168
14. **Pochampally RR, Neville BT, Schwarz EJ, Li MM, Prockop DJ** 2004 Rat adult stem cells (marrow stromal cells) engraft and differentiate in chick embryos without evidence of cell fusion. Proc Natl Acad Sci USA 101:9282–9285
15. **Makino S, Fukuda K, Miyoshi S, Konishi F, Kodama H, Pan J, Sano M, Takahashi T, Hori S, Abe H, Hata J, Umezawa A, Ogawa S** 1999 Cardiomyocytes can be generated from marrow stromal cells in vitro. J Clin Invest 103:697–705
16. **Okamoto T, Aoyama T, Nakayama T, Nakamata T, Hosaka T, Nishijo K, Nakamura T, Kiyono T, Toguchida J** 2002 Clonal heterogeneity in differentiation potential of immortalized human mesenchymal stem cells. Biochem Biophys Res Commun 295:354–361
17. **Hu MC, Chou SJ, Huang YY, Hsu NC, Li H, Chung BC** 1999 Tissue-specific, hormonal, and developmental regulation of SCC-LacZ expression in transgenic mice leads to adrenocortical zone characterization. Endocrinology 140: 5609–5618
18. **Mizutani T, Yamada K, Yazawa T, Okada T, Minegishi T, Miyamoto K** 2001 Cloning and characterization of gonadotropin-inducible ovarian transcription factors (GIOT1 and -2) that are novel members of the (Cys)(2)-(His)(2)-type zinc finger protein family. Mol Endocrinol 15:1693–1705
19. **Rutledge RG, Cote C** 2003 Mathematics of quantitative kinetic PCR and the application of standard curves. Nucleic Acids Res 31:e93
20. **Yazawa T, Mizutani T, Yamada K, Kawata H, Sekiguchi T, Yoshino M, Kajitani T, Shou Z, Miyamoto K** 2003 Involvement of cyclic adenosine 5′-monophosphate response element-binding protein, steroidogenic factor 1, and Dax-1 in the regulation of gonadotropin-inducible ovarian transcription factor 1 gene expression by follicle-stimulating hormone in ovarian granulosa cells. Endocrinology 144:1920–1930
21. **Bose HS, Whittal RM, Baldwin MA, Miller WL** 1999 The active form of the steroidogenic acute regulatory protein, StAR, appears to be a molten globule. Proc Natl Acad Sci USA 96:7250–7255
22. **Hu MC, Guo IC, Lin JH, Chung BC** 1991 Regulated expression of cytochrome P-450scc (cholesterol-side-chain cleavage enzyme) in cultured cell lines detected by antibody against bacterially expressed human protein. Biochem J 274(Pt 3):813–817
23. **Hales DB, Sha LL, Payne AH** 1987 Testosterone inhibits cAMP-induced *de novo* synthesis of Leydig cell cytochrome P-450($17\alpha$) by an androgen receptor-mediated mechanism. J Biol Chem 262:11200–11206
24. **Medvinsky A, Smith A** 2003 Stem cells: fusion brings down barriers. Nature 422:823–825
25. **O'Shaughnessy PJ, Willerton L, Baker PJ** 2002 Changes in Leydig cell gene expression during development in the mouse. Biol Reprod 66:966–975
26. **Parker KL, Schimmer BP** 1997 Steroidogenic factor 1: a key determinant of endocrine development and function. Endocr Rev 18:361–377
27. **Peng L, Arensburg J, Orly J, Payne AH** 2002 The murine $3\beta$-hydroxysteroid dehydrogenase ($3\beta$-HSD) gene family: a postulated role for $3\beta$-HSD VI during early pregnancy. Mol Cell Endocrinol 187:213–221
28. **Staels B, Hum DW, Miller WL** 1993 Regulation of steroidogenesis in NCI-H295 cells: a cellular model of the human fetal adrenal. Mol Endocrinol 7:423–433
29. **Heim M, Frank O, Kampmann G, Sochocky N, Pennimpede T, Fuchs P, Hunziker W, Weber P, Martin I, Bendik I** 2004 The phytoestrogen genistein enhances osteogenesis and represses adipogenic differentiation of human primary bone marrow stromal cells. Endocrinology 145:848–859
30. **Lo KC, Lei Z, Rao Ch V, Beck J, Lamb DJ** 2004 *De novo* testosterone production in luteinizing hormone receptor knockout mice after transplantation of Leydig stem cells. Endocrinology 145:4011–4015
31. **De Bari C, Dell'Accio F, Tylzanowski P, Luyten FP** 2001 Multipotent mesenchymal stem cells from adult human synovial membrane. Arthritis Rheum 44:1928–1942
32. **Crawford PA, Sadovsky Y, Milbrandt J** 1997 Nuclear receptor steroidogenic factor 1 directs embryonic stem cells toward the steroidogenic lineage. Mol Cell Biol 17:3997–4006
33. **Bjorkhem I** 2002 Do oxysterols control cholesterol homeostasis? J Clin Invest 110:725–730
34. **Pandak WM, Ren S, Marques D, Hall E, Redford K, Mallonee D, Bohdan P, Heuman D, Gil G, Hylemon P** 2002 Transport of cholesterol into mitochondria is rate-limiting for bile acid synthesis via the alternative pathway in primary rat hepatocytes. J Biol Chem 277:48158–48164
35. **Gondo S, Yanase T, Okabe T, Tanaka T, Morinaga H, Nomura M, Goto K, Nawata H** 2004 SF-1/Ad4BP transforms primary long-term cultured bone marrow cells into ACTH-responsive steroidogenic cells. Genes Cells 9:1239–1247

*Endocrinology* is published monthly by The Endocrine Society (http://www.endo-society.org), the foremost professional society serving the endocrine community.

ARTICLE

doi:10.1016/j.ymthe.2005.09.020

# Histopathological and Behavioral Improvement of Murine Mucopolysaccharidosis Type VII by Intracerebral Transplantation of Neural Stem Cells

Yasuyuki Fukuhara,[1,2] Xiao-Kang Li,[3] Yusuke Kitazawa,[3] Masumi Inagaki,[4] Kentaro Matsuoka,[5] Motomichi Kosuga,[1] Rika Kosaki,[1,2] Takuya Shimazaki,[6] Hitoshi Endo,[7] Akihiro Umezawa,[8] Hideyuki Okano,[6] Takao Takahashi,[2] and Torayuki Okuyama[1,2,*]

[1]*Department of Clinical Genetics and Molecular Medicine,* [3]*Department of Innovative Surgery,* [8]*Department of Reproductive Biology, and* [5]*Department of Pathology, National Center for Child Health and Development, 2-10-1 Okura, Setagaya-ku, Tokyo 157-8535, Japan*
[2]*Department of Pediatrics and* [6]*Department of Physiology, Keio University School of Medicine, 35 Shinanomachi, Shinjuku-ku, Tokyo 160-8582, Japan*
[4]*National Center of Neurology and Psychiatry, 1-7-1 Koumodai, Ichikawa-shi, Chiba 272-8516, Japan*
[7]*Biochemistry of Experimental Medicine, Jichi Medical School, Minamikawachi-machi, Kawachi-gun, Tochigi 329-0498, Japan*

**To whom correspondence and reprint requests should be addressed. Fax: +81 3 3416 2222. E-mail: okuyama-t@ncchd.go.jp.*

Available online 28 November 2005

**The therapeutic efficacy of neural stem cell transplantation for central nervous system (CNS) lesions in lysosomal storage disorders was explored using a murine model of mucopolysaccharidosis type VII (MPS VII). We used fetal neural stem cells derived from embryonic mouse striata and expanded *in vitro* by neurosphere formation as the source of graft materials. We transplanted neurospheres into the lateral ventricles of newborn MPS VII mice and found that donor cells migrated far beyond the site of injection within 24 h, and some of them could reach the olfactory bulb. A quantitative measurement indicated that the GUSB activity in the brain was 12.5 to 42.3% and 5.5 to 6.3% of normal activity at 24 h and 3 weeks after transplantation. In addition, histological analysis revealed a widespread decrease in lysosomal storage in the recipient's hippocampus, cortex, and ependyma. A functional assessment with novel-object recognition tests confirmed improvements in behavioral patterns. These results suggest that intracerebral transplantation of neural stem cells is feasible for treatment of CNS lesions associated with lysosomal storage disorders.**

**Key Words: neurosphere, mucopolysaccharidosis type VII, intracerebral transplantation**

## INTRODUCTION

Mucopolysaccharidosis type VII (MPS VII), or Sly syndrome, is a congenital lysosomal storage disorder (LSD) characterized by a systemic deficiency of β-glucuronidase (GUSB) activity [1]. This defect results in a progressive accumulation of undegraded glycosaminoglycans and subsequent lysosomal distension in multiple tissues, including the central nervous system (CNS). Enzyme replacement therapy and bone marrow transplantation are effective for correcting visceral manifestations of the disorder [2,3]. However, effective treatment of the CNS in patients with LSDs remains a major challenge.

With respect to cell therapy directed to the CNS in an MPS VII mouse, there are reports that the intracerebral transplantation of a genetically engineered neural progenitor [4] and retrovirally transduced syngeneic fibroblasts [5] corrected the lysosomal storage of the recipient's brain tissues. We also previously reported that adeno virally transduced rat amniotic epithelial cells injected into adult MPSVII mouse brains survived at the injection point for more than 9 weeks and the subsequent supply of enzyme resulted in pathological improvement in multiple areas of the MPS VII mouse brains [6].

In this study, we used fetal neural stem cells derived from embryonic mouse striata and expanded *in vitro* by neurosphere formation [7,8] as the source of graft materials. Neural stem cells are considered to be good candidates for cell therapy to treat CNS dysfunction. In fact, fetal neural tissues have been successfully used in human Parkinson disease patients [9,10]; however, as many as four to eight fetuses were required to obtain a sufficient number of cells to treat a single patient. Expansion of neural stem cells *in vitro* may overcome the above practical

*Abbreviations used:* CNS, central nervous system; GUSB, β-glucuronidase; MPS VII, mucopolysaccharidosis type VII.



1525-0016/$30.00

and ethical problems associated with fetal tissue transplantation and provide a source for graft material.

Here we describe improvements in the histopathology of the hippocampus, cortex, and ependyma and in non-spatial hippocampus-dependent learning and memory evaluated in a novel-object recognition test at 2 months after transplantation. These data suggest that early transplantation of neurospheres into the CNS may prevent or delay some of the progressive mental impairment associated with this LSD.

## Results and Discussion

### Production and Secretion Capacity of GUSB Enzymes by Neurospheres

The neurosphere is a floating cell cluster containing plenty of neural stem cells and is generated from a fetal mouse brain by neurosphere formation [7,8]. Briefly, when we culture fetal corpus striatum containing neural stem cells in a serum-free medium with growth factors, only neural stem cells can survive and form floating cell clusters called neurospheres. We initially determined the endogenous GUSB activity of neurospheres obtained from normal C57BL/6 mice. The GUSB activity of the neurosphere and its culture medium proved significantly higher than that of bone marrow cells (Figs. 1A and 1B). We also evaluated the difference in GUSB activity before and after differentiation. Most neurospheres differentiate into neural cells *in vivo* according to their microenvironments after transplantation [8]. The GUSB activities in differentiated cells and their culture media were almost equivalent to those of bone marrow cells, suggesting that the GUSB activity of the neurospheres was reduced, although it was maintained to the extent necessary for a therapeutic effect even after differentiation.

### Intercellular Transport of the GUSB Enzyme

It is well known that most lysosomal enzymes can be taken up into cells by M6P receptor-mediated endocytosis, and that this process is efficiently blocked in the presence of M6P [11]. When we transferred the culture medium of neurospheres generated from C57BL/6 fetal mouse brains to dishes of the primary culture of neurons generated from C3H mice, 21.9% of the heat-stable C57BL/6 mouse-derived GUSB in the culture medium was internalized into the neurons in the absence of M6P (Fig. 1C). In contrast, it was significantly reduced in the presence of 10 mM M6P (Fig. 1C). This suggests that endocytosis by M6P receptors leads to the internalization of the GUSB enzyme secreted from the neurospheres to the neurons.

### Lysosomal Enzyme Activities of the Neurosphere

Many LSDs display CNS symptoms. Most lysosomal enzymes have common transport systems mediated by the M6P receptor, and therefore the same transplantation strategy could be available if neurospheres can produce and secrete significant amounts of lysosomal enzymes. We determined the specific activities of several lysosomal enzymes in neurospheres and compared them with those in marrow stromal cells and human granulocytes. Similar or higher activities of lysosomal enzymes were identified in the neurosphere (Table 1).

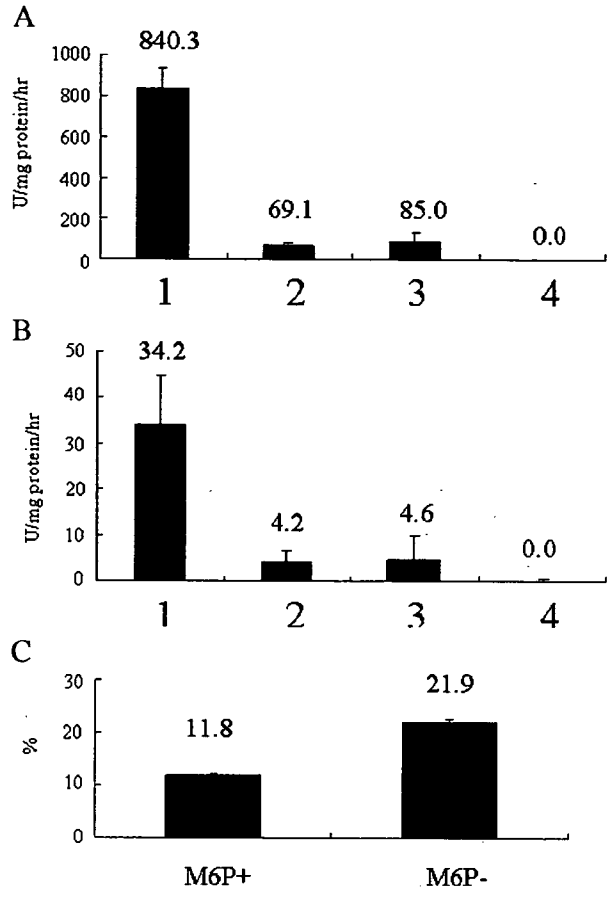


FIG. 1. Neurosphere GUSB activities and secretion via cell-to-cell transport. Lanes 1, neurospheres; 2, differentiated cells from neurospheres; 3, bone marrow cells; 4, 3521 cells (fibroblasts that originated from an MPS VII mouse). The GUSB activities of the neurosphere and its culture medium proved significantly higher than those of bone marrow cells. The GUSB activity in differentiated cells from neurospheres and that of its culture medium were almost equivalent to those of bone marrow cells. (A) GUSB activity in cell pellets of the neurosphere, bone marrow, and 3521 cells. (B) GUSB activity in a culture medium of the neurosphere, bone marrow, and 3521 cells at the time of the first passage. (C) Cell-to-cell transport of GUSB secreted from neurospheres. The ratio of the heat-stable GUSB activity in C3H mouse neural cells to the total heat-stable GUSB activity in the culture medium was calculated. The means ± standard errors are provided.

### Distribution of Donor Cells after Neonatal Transplantation

We performed a syngeneic transplantation experiment using neurospheres obtained from CAG-EGFP transgenic

doi:10.1016/j.ymthe.2005.09.020

**TABLE 1:** Activities of lysosomal enzymes in the neurosphere and their related diseases[a]

| Lysosomal enzyme | Disease | Neurosphere | MSC[b] | Granulocytes |
|---|---|---|---|---|
| α-L-Iduronidase | MPS I | 39.2 | 57.4 | 56–201 ($n$ = 6) |
| Iduronate sulfatase | MPS II | 40.5 | 20 | 12–26 ($n$ = 5) |
| Heparan-*N*-sulfatase | MPS IIIA | 1.1 | 4.3 | 0.2–3 ($n$ = 4) |
| GalNAc-6-*S*-sulfatase | MPS IVA | 5.3 | 15.2 | 8.1–20 ($n$ = 5) |
| Arylsulfatase B | MPS VI | 55.3 | 15.5 | 9–32 ($n$ = 5) |
| β-Glucosidase | Gaucher disease | 3.0 | 6.5 | 0.2–0.6 ($n$ = 100) |
| α-Galactosidase A | Fabry disease | 189 | 68.8 | 49.8–116.4 ($n$ = 48) |
| β-Galactosidase | MPS IVB | 501 | 309 | 37.6–230.1 ($n$ = 100) |
| α-Mannosidase | α-Mannosidosis | 61.0 | 48.0 | 121.1–345.1 ($n$ = 100) |
| β-Hexosaminidase | Sandhoff disease | 1024 | 3062 | 401.7–1426.0 ($n$ = 100) |
| β-Hexosaminidase A | Tay–Sachs disease | 527 | 481 | 251.1–607.4 ($n$ = 48) |
| Arylsulfatase A | MLD | 435 | 278 | 109.0–217.2 ($n$ = 100) |

[a] We quantitatively assayed for a variety of lysosomal enzymes as well as GUSB. Several kinds of lysosomal enzymes were found to be high in the neurosphere. This result suggests that the neurosphere may be applied for the treatment of different types of congenital metabolic disorder. Data are given in nmol/mg protein/h. Enzyme activities in human granulocytes were measured as described elsewhere [27].
[b] MSC, marrow stromal cell.

mice (C57BL/6 background) as donor cells and newborn MPS VII mice as recipients. We injected 2.5–5 × $10^4$ neurospheres (Fig. 2A) into the lateral ventricles of neonatal MPS VII mice within 1 to 3 days after delivery. A large number of donor cells were located mainly in the periventricular area at the hippocampus level in the brain, but a small number of GFP-positive cells were observed at varying distances away from the periventricular area at 24 h (Fig. 2B). We identified some of the GFP-positive cells in a linear formation at the level of the olfactory bulb, indicating a specific manner of migration in this area that is referred to as chain migration [12] (Fig. 2C). The overall distribution of the donor cells throughout the brain was essentially identical in all mice examined histologically ($n$ = 3), with findings similar to previous reports [4,13–15]. There was evidence of GUSB

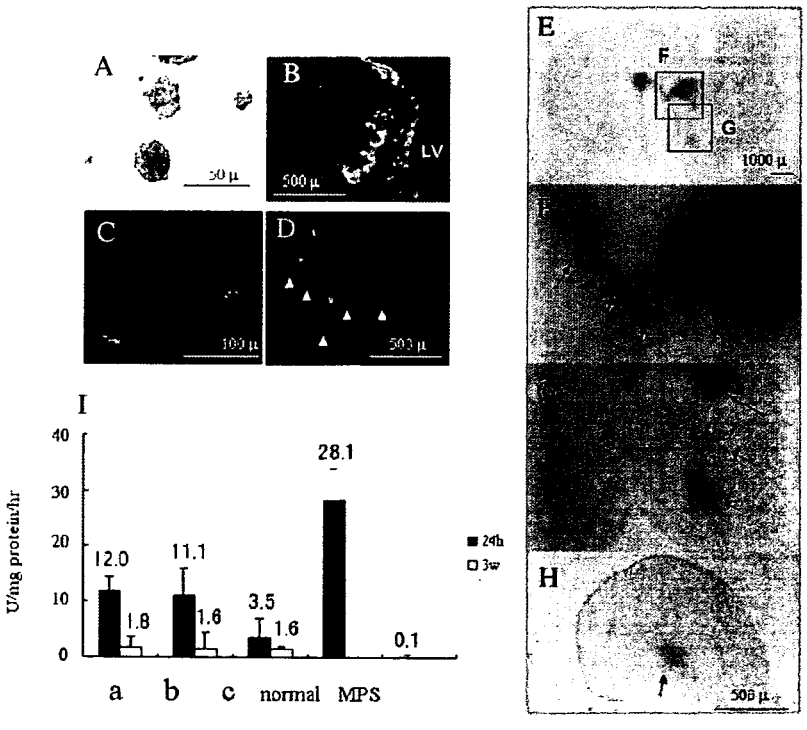


FIG. 2. Distribution of the donor cells in a mouse brain following transplantation of neurospheres. (A) Neurospheres generated from GFP transgenic mice under a fluorescence microscope. (B) A slice at the hippocampus level in the brain at 24 h after transplantation under a fluorescence microscope. GFP-positive cells were located mainly in the periventricular area. (C) A slice at the olfactory bulb level in the brain at 24 h after transplantation. GFP-positive cells were also detected under a fluorescence microscope; some of them were found to form a line (a chain migration). (D) A slice at the hippocampus level in the brain under a fluorescence microscope at 3 weeks after transplantation. GFP-positive cells were found to be branched and to form a network with the recipient brain tissue. (E–H) The brain of an MPS VII mouse at 24 h after transplantation of neurospheres. The recipient brain was stained red by GUSB staining in accordance with the GFP-positive area. (E–G) Coronal sections of the telencephalon at the caudal level. (H) Olfactory bulb. (I) Quantitative determination of the GUSB activity was performed at 24 h and 3 weeks after transplantation. The brains of the transplant recipients were divided coronally into three parts and quantitatively assayed for GUSB activity ($n$ = 3). The regions used for evaluation at the designated times were defined by anatomical landmarks in the anterior-to-posterior plane: a, olfactory bulbs; b, caudal edge of the olfactory bulbs to the rostral edge of the hippocampus; c, hippocampus to the posterior colliculus. The cerebellum was dissected free and was not included in the assay.

staining in accordance with the GFP-positive area, indicating a rise in GUSB activity (Figs. 2E–2H).

We previously reported that neurosphere-derived donor neurons extend their processes into the host tissues and form a synaptic structure [8]. The GFP-positive cells had extended their processes and formed synaptic structures as well 3 weeks after transplantation (Fig. 2D). These data suggest that the donor cells migrated from the periventricular area and some of them reached the olfactory bulb as early as 24 h after transplantation.

### Quantitative Gusb Assay in Transplanted Mouse Brains

We divided the brains of the transplant recipients coronally into three parts and quantitatively assayed them for GUSB activity at 24 h ($n$ = 3) and 3 weeks ($n$ = 3) after transplantation (Fig. 2I). GUSB activity was 12.5 to 42.3% of normal activity at 24 h. There was 5.5 to 6.3% of normal activity at 3 weeks after transplantation. This is an amount at which that lysosomal distensions in the neuron and glia could also be reversed [16]. These results imply that donor cells provided the recipient brain with GUSB activity to the extent that lysosomal storage in the recipient brain could be prevented for at least 3 weeks.

### Histological Analysis and Tumorigenesis Assessment of the Treated Mice

We tested the treated MPS VII mice for reduction of lysosomal distensions in the neurons and glia at 2 months after transplantation ($n$ = 2) (Figs. 3 and 4). We performed a histological analysis on hippocampus, cortex, and ependyma using an optical microscope (hippocampus, cortex, and ependyma) and an electron microscope (cortex). In the hippocampus of the untreated MPS VII mice, most of neurons contained marked cytoplasmic vacuolation (lysosomal storage) as well as astrocytes. In contrast, those of the treated hippocampuses were almost eliminated especially from neurons in this area. In the cortices, we also observed extensive neuronal and glial vacuolation, and the treatment reduced them remarkably as well. An electron microscope demonstrated that lysosomal storage in some neurons was completely eliminated in this area

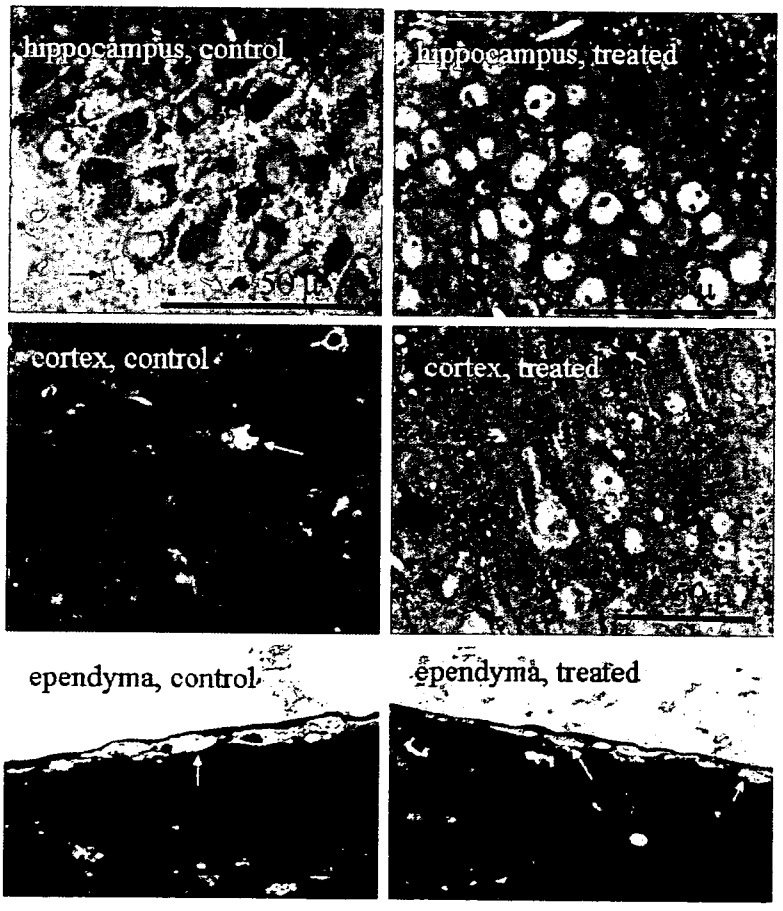


FIG. 3. Toluidine blue-stained, 0.5-μm-thick sections from the hippocampus, cortex, and ependyma are from 2-month-old MPS VII mice ($n$ = 2). Intraventricular injection of neurospheres decreases lysosomal storage in the hippocampus, cortex, and ependyma. Black arrows indicate distended vacuoles in neurons; white arrows indicate storage in glia.

doi:10.1016/j.ymthe.2005.09.020

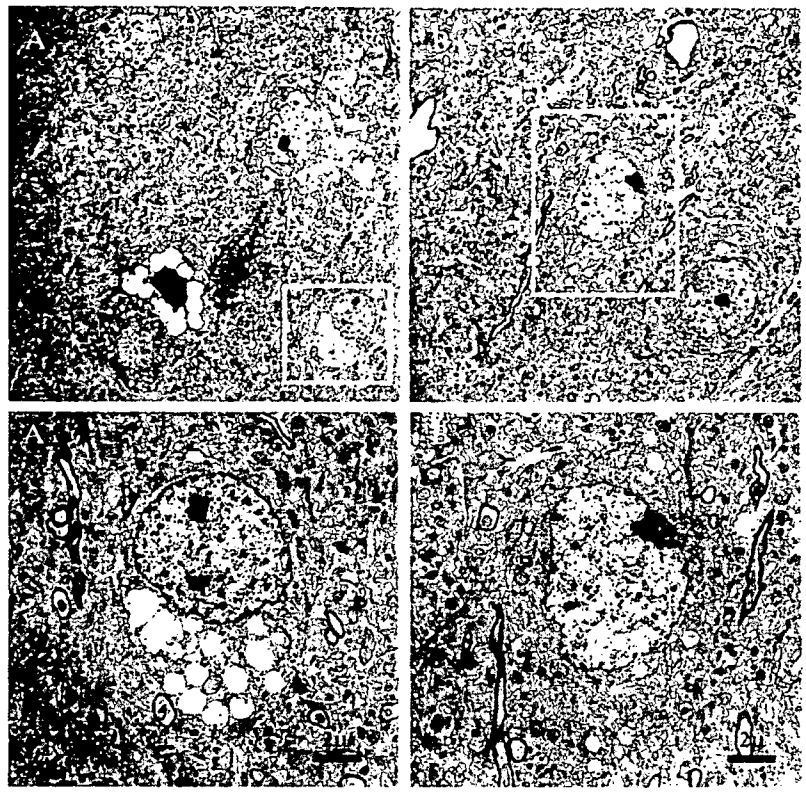

FIG. 4. Electron microscopic analysis of lysosomal storage in a mouse brain following transplantation of neurospheres. (A) Cortex of a control untreated MPS VII mouse at 2 months after transplantation. Abundant white cytoplasmic vacuoles represent distended lysosomes. (B) Cortex of a MPS VII mouse at 2 months after transplantation. Lysosomal storage granules in this area were remarkably reduced in size and number, and those in some neurons were completely eliminated. (A′ and B′) Magnified photographs of the circumscribed areas in (A) and (B).

(Fig. 4). In the ependyma, the amount of storage appeared to be significantly reduced in the treated mice. To evaluate quantitatively the improvement of the pathology in the treated mice, we counted neurons and glia containing apparent vacuolation in each hippocampus and cortex of the treated and the untreated mice ($n = 2$, total 300 cells in each area) in the HPF (×600). In both areas, we observed a remarkable decrease in the number of neurons and glia with apparent lysosomal storage, and this finding was almost equal in two treated mice, indicating an improvement of the pathology in the treated mouse brains (Table 2). We carefully assessed all transplanted mice for the presence of tumorigenesis. We dissected the brains of the dead mice during the course of the study and macroscopically analyzed them for tumor formation, but we could not identify any tumor formation among them.

**TABLE 2:** The percentage of cells with apparent vacuolization in the brain of MPS VII mice treated with intraventricular injection of neurospheres[a] ($n = 2$)

| | Untreated | Treated |
|---|---|---|
| Hippocampus | 89.3% | 17.3% |
| Neuron | 90% | 18.4% |
| Glia | 92% | 13.9% |
| Cortex | 42% | 15.3% |
| Neuron | 37.7% | 11.7% |
| Glia | 55.6% | 30% |

[a] Toluidine blue sections of hippocampus and cortex were analyzed for lysosomal distention, and we counted neurons and glia containing much vacuolation in 300 cells in each of hippocampus and cortex in the HPF (×600).

### Mouse Hearing Acuity Assessment

Measurements of the auditory brain-stem response (ABR) have been useful in assessing functional improvements after treatment [17]. We tested three treated MPS VII mice, three untreated MPS VII mice, and three C57BL/6 mice. There was no significant difference in the ABR thresholds among the treated and the untreated MPS VII mice (Fig. 5A). It is well known that malalignment and focal loss of stereocilia occur as the disease progresses, leading to a sensorineural hearing loss [18]. As the ABR was performed at 2 months, it may have been too early to assess the sensorineural hearing loss.

### Behavioral Assessment

We used a novel-object recognition test, a tool for studying nonspatial hippocampus-dependent memory, to determine whether an improvement in mental status could be achieved by transplantation [19–21]. We carried out this test as described [19] with several modifications at 2 months after transplantation ($n = 3$). We used normal siblings of the treated MPS VII mice as the control mice. In summary, after the mice were habituated to an open field, two yellow objects (A, B) were placed diagonally in

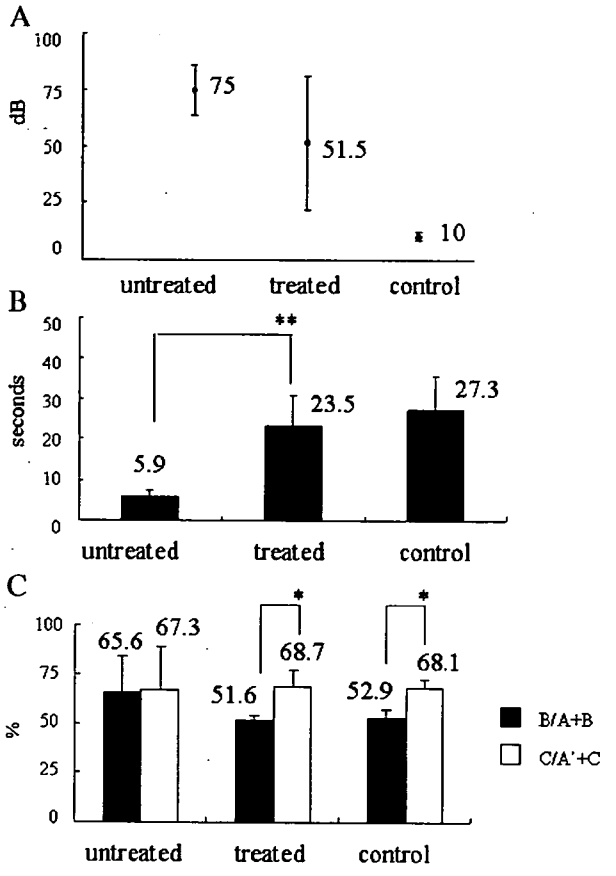


FIG. 5. Assessment of the functional recovery at 2 months after transplantation. (A) Auditory-evoked brain-stem responses. The decibels required to elicit ABR at the broadband (clicks) were evaluated among three normal mice, three treated MPS VII mice, and three untreated MPS VII mice at 2 months after transplantation. There was no significant difference in the ABR thresholds among the treated MPS VII mice and the untreated MPS VII mice. (B) The novel-object recognition test. The mice were assessed for an improvement in hippocampus-dependent nonspatial memory by a novel-object recognition test ($n = 3$). The total time spent exploring objects on day 4 (=A + B) in the treated mice was significantly longer than that for the untreated mice. (**$P < 0.01$). (C) The novel-object recognition test (retention test). The percentage of time spent in exploring B as a portion of the total object exploration time on day 4 [B/(A + B)] was compared with that of C (the novel object) on day 5 [C/(A′ + C)]. C/(A′ + C) in the C57BL/6 and the treated mice was significantly greater than B/(A + B). This suggests that the normal mice and the treated mice spent a significantly longer time exploring the novel object, revealing that both groups had a significant preference for exploring the novel object. The means ± standard errors are provided.

the open field on day 4, and the mice were allowed to explore them for 10 min. Object B was replaced with a novel object (C) and the other object was replaced with a replica (A′) on day 5, and the mice were again allowed to explore them for 10 min. Normal animals prefer to explore the novel object more than the familiar object. From the degree of preference for exploration of the new object, it can be inferred that they retained a memory of the familiar object. The total time spent exploring object A or B on day 4 (=A + B) was 27.3 ± 8.4 s in the normal mice, 23.5 ± 7.4 s in the treated mice, and 5.9 ± 1.6 s in the untreated mice (Fig. 5B), indicating that the normal and the treated mice had the same levels of motivation, curiosity, and interest in exploring objects. Next, to evaluate preferential exploration of the novel object, we compared the percentage of time spent exploring object B as a portion of the total object-exploration time on day 4 [=B/(A + B)] with that of object C (the novel object) on day 5 [=C/(A′ + C)] (Fig. 5C). C/(A′ + C) in the normal and the treated mice was significantly greater than B/(A + B) [normal mice, B/(A + B) = 52.9 ± 3.9%, C/(A′ + C) = 68.1 ± 4.4%; treated mice, B/(A + B) = 51.6 ± 2.8%, C/(A′ + C) = 68.7 ± 8.4% of the exploration time]. This indicates that the normal mice and the treated mice spent a significantly longer time exploring the novel object, revealing that both groups exhibited a significant preference for exploring it. These results indicate that the treated mice have the same level of nonspatial hippocampus-dependent memory as the normal mice. But we cannot completely deny the possibility that the vision had an influence on this improvement of a novel object test.

To date, there are reports demonstrating an improvement in behavior of treated MPS VII mice assessed by a Morris water maze test [22,23]. We used a novel-object test because it is very easy and less of a burden on the mice than the Water maze test. Consequently, it is easily applicable to mice with motility disturbance, and we thought we could maximize mouse performance associated with visual recognition memory. The long-term effects of this treatment have not been examined in detail. The treated mice lived to 7 months of age at most. Transplantation of neurospheres did not extend the life span of MPS VII mice. Life span may be dependent on systemic lysosomal storage other than the CNS.

In summary, our results demonstrated that after transplantation of *in vitro*-expanded neurospheres into the neonatal ventricle of MPS VII mice brains, the transplant donor cells migrated along established routes and integrated into the recipient's brain. The treated mice exhibited improved cognitive functions as measured by a novel-object recognition test, which was consistent with histological evidence of reduced lysosomal storage in the brain tissue.

## Materials and Methods

***Animals.*** Syngeneic MPS VII (*mps/mps*) mice were obtained from a pedigree colony of B6.C-H-$2^{bml}$/ByBir-gus$^{mps}$/+ mice maintained at our facility [6]. Normal C3H mice were purchased from Shizuoka Laboratory Animal Center (Shizuoka, Japan). CAG-EGFP transgenic mice were originally generated by Endo *et al.* [24,25]. All mice were maintained and treated in accordance with the guidelines of the animal committee of the facility.

***Isolation, primary cultures, and passaging procedures of neurospheres.*** Embryos were removed from CAG-EGFP transgenic mice on day 14.5 of pregnancy. The corpus striatum was dissected and prepared as described

doi:10.1016/j.ymthe.2005.09.020

elsewhere [7]. Neurospheres were cultured in the medium described below at 37°C with 5% $CO_2$ at a concentration of $2 \times 10^5$ cells/ml in the primary culture. The culture medium was DMEM/F12 supplemented with the hormone mixture used by Reynolds and Weiss [7]. Passages were performed once per week. Neurospheres were used for the transplantation after the second to fifth passage.

***Cell-to-cell transport of GUSB secreted from neurospheres.*** We evaluated *in vitro* the uptake ratio of the GUSB enzyme secreted from neurospheres of C57BL/6 mice into neural cells of C3H mice by using the difference in the heat stability of GUSB proteins between C57BL/6 mice and C3H mice. In brief, GUSB activity of C57BL/6 mice was reduced by only 30% after a 2-h incubation at 65°C [11]. In contrast, GUSB activity of C3H mice was decreased markedly after this procedure. We prepared a culture medium of neurospheres from C57BL/6 mice after 1 week incubation. We replaced the medium of primary neurons of C3H mice with the above medium, continued to culture in the presence or absence of M6P, and harvested 12 h later. Heat-stable GUSB activity in the homogenates of C3H mouse neurons was measured after a 2-h incubation at 65°C.

***Quantitative analysis of GUSB activity.*** GUSB activity in tissues and cell homogenates was quantified using a fluorometric assay described previously [26]. Neurospheres were quantitatively analyzed after the second to fifth passage. Differentiated cells were obtained from neurospheres by converting the culture medium into DMEM +10% FBS. We had previously demonstrated that these cells differentiated into neurons, astrocytes, and oligodendrocytes by immunological staining (data not shown). Bone marrow was isolated from C57BL/6 mice and cultured in DMEM +10% FBS. Attached cells were collected after the second to fifth passage and analyzed for GUSB activity.

***Histochemical detection of GUSB activity.*** The mice were perfused with physiological saline and subsequently with 4% paraformaldehyde before preparation of the brains. The brains were equilibrated in a 30% sucrose solution (4°C, overnight), frozen in M-1 embedding matrix (Shandon, Pittsburgh, PA, USA), and then sectioned on a cryostat. Histochemical analysis of GUSB activity was performed on 20-μm-thick frozen sections using naphthol AS-BI β-D-glucuronide (Sigma) as a substrate [26].

***Lysosomal enzyme activities of the neurosphere.*** Lysosomal enzyme activities in neurospheres, the marrow stromal cells, and human granulocytes were quantified using a fluorometric assay as described with some modification [27].

***Histopathological analysis of lysosomal storage.*** Histopathology in neurons and glia was analyzed at 2 months after transplantation, corresponding to 2 months of age ($n = 2$). Tissues were isolated from the mice and immediately immersed in cold 2% glutaraldehyde in 0.1 M cacodylate buffer, postfixed in 1% osmium tetroxide, dehydrated through a graded series of ethanol solutions, and embedded in Spurr's Medium (Polyscience, Warrington, PA, USA). Toluidine blue-stained, 0.5-μm-thick sections were analyzed for evidence of lysosomal storage in hippocampus, cortex, and ependyma. Cytoplasmic lysosomal distensions in the cortex were also evaluated with an electron microscope.

***Auditory brain-stem responses.*** ABR examination was performed 20 min after anesthesia in a quiet room, as described previously [28].

***Novel-object recognition tests.*** Novel-object recognition tests evaluate nonspatial hippocampus-dependent learning and memory [19–21] and were performed as described [19] with several modifications. The mice were habituated in an open field over a 2-day preexposure (day 1 for 5 min and day 3 for 5 min). Two yellow objects (A and B) were placed diagonally in the open field (15 cm away from the walls) on day 4, and the mice were allowed to explore them for 10 min. Object B was replaced with the novel object (C), and the other object was replaced with a replica (A′) on day 5, and the mice were again allowed to explore them for 10 min. Recognition of the familiar object was scored by preferential exploration of the novel object. A + B represents total time exploring on day 4. A′ + C represents total time exploring on day 5. B/(A + B) represents the ratio of time exploring object B to total time exploring on day 4. C/(A′ + C) represents the ratio of time exploring object C to total time exploring on day 5.

## ACKNOWLEDGMENTS

*This work was supported by a grant from Terumo Foundation Life Science Foundation to HO, and a grant from the 21st Century COE program of the Japanese Ministry of Education, Culture, Sports, Science and Technology Ministry to Keio University.*

RECEIVED FOR PUBLICATION APRIL 27, 2005; REVISED SEPTEMBER 13, 2005; ACCEPTED SEPTEMBER 27, 2005.

## REFERENCES

1. Sly, W. S., Quinton, B. A., McAllister, W. H., and Rimoin, D. L. (1973). β-Glucuronidase deficiency: report of clinical, radiologic, and biochemical features of a new mucopolysaccharidosis. *J. Pediatr.* **82:** 249–257.
2. Vogler, C., *et al.* (1993). Enzyme replacement with recombinant beta-glucuronidase in the newborn mucopolysaccharidosis type VII mouse. *Pediatr. Res.* **34:** 837–840.
3. Birkenmeier, E. H., *et al.* (1991). Increased life span and correction of metabolic defects in murine mucopolysaccharidosis type VII after syngeneic bone marrow transplantation. *Blood* **78:** 3081–3092.
4. Snyder, E. Y., Taylor, R. M., and Wolfe, J. H. (1995). Neural progenitor cell engraftment corrects lysosomal storage throughout the MPS VII mouse brain. *Nature* **374:** 367–370.
5. Taylor, R. M., and Wolfe, J. H. (1997). Decreased lysosomal storage in the adult MPS VII mouse brain in the vicinity of grafts of retroviral vector-corrected fibroblasts secreting high levels of β-glucuronidase. *Nat. Med.* **3:** 771–775.
6. Kosuga, M., *et al.* (2001). Engraftment of genetically engineered amniotic epithelial cells corrects lysosomal storage in multiple areas of the brain in mucopolysaccharidosis type VII mice. *Mol. Ther.* **3:** 139–148.
7. Reynolds, B. A., and Weiss, S. (1992). Generation of neurons and astrocytes from isolated cells of adult mammalian central nervous system. *Science* **255:** 1707–1710.
8. Ogawa, Y., *et al.* (2002). Transplantation of in vitro-expanded fetal neural progenitor cells results in neurogenesis and functional recovery after spinal cord contusion injury in adult rats. *J. Neurosci. Res.* **69:** 925–933.
9. Lindvall, O., *et al.* (1990). Grafts of fetal dopamine neurons survive and improve motor function in Parkinson's disease. *Science* **247:** 574–577.
10. Freed, C. R., *et al.* (1992). Survival of implanted fetal dopamine cells and neurologic improvement 12 to 46 months after transplantation for Parkinson's disease. *N. Engl. J. Med.* **327:** 1549–1555.
11. Gwynn, B., Lueders, K., Sands, M., and Birkenmeier, E. H. (1998). Intracisternal A-particle element transposition into the murine β-glucuronidase gene correlates with loss of enzyme activity: a new model for β-glucuronidase deficiency in the C3H mouse. *Mol. Cell. Biol.* **18:** 6474–6481.
12. Lois, C., and Alvarez-Buylla, A. (1994). Long-distance neuronal migration in the adult mammalian brain. *Science* **264:** 1145–1148.
13. Ourednik, V., *et al.* (2001). Segregation of human neural stem cells in the developing primate forebrain. *Science* **293:** 1820–1824.
14. Meng, X. L., Shen, J. S., Ohashi, T., Maeda, H., Kim, S. U., and Eto, Y. (2003). Brain transplantation of genetically engineered human neural stem cells globally corrects brain lesions in the mucopolysaccharidosis type VII mouse. *J. Neurosci. Res.* **74:** 266–277.
15. Tamaki, S., *et al.* (2002). Engraftment of sorted/expanded human central nervous system stem cells from fetal brain. *J. Neurosci. Res.* **69:** 976–986.
16. Sferra, T. J., Backstorm, K., Wang, C., Rennard, R., Miller, M., and Hu, Y. (2004). Widespread correction of lysosomal storage following intrahepatic injection of a recombinant adeno-associated virus in the adult MPS VII mouse. *Mol. Ther.* **10:** 478–491.
17. Kopen, G. C., Prockop, D. J., and Phinney, D. G. (1999). Marrow stromal cells migrate throughout forebrain and cerebellum, and they differentiate into astrocytes after injection into neonatal mouse brains. *Proc. Natl. Acad. Sci. USA* **96:** 10711–10716.
18. Sands, M. S., Erway, L. C., Vogler, C., Sly, W. S., and Birkenmeier, E. H. (1995). Syngeneic bone marrow transplantation reduces the hearing loss associated with murine mucopolysaccharidosis type VII. *Blood* **86:** 2033–2040.
19. Dulawa, S. C., Grandy, D. K., Low, M. J., Paulus, M. P., and Geyer, M. A. (1999). Dopamine D4 receptor-knock-out mice exhibit reduced exploration of novel stimuli. *J. Neurosci.* **19:** 9550–9556.
20. Soderling, S. H., *et al.* (2003). Loss of Wave-1 causes sensorimotor retardation and reduced learning and memory in mice. *Proc. Natl. Acad. Sci. USA* **100:** 1723–1728.
21. Rompon, C., *et al.* (2000). Enrichment induces structural changes and recovery from nonspatial memory deficits in CA1 NMDAR-knockout mice. *Nat. Neurosci.* **3:** 238–244.
22. O'Connor, L. H., *et al.* (1998). Enzyme replacement therapy for murine mucopolysaccharidosis type VII leads to improvements in behavior and auditory function. *J. Clin. Invest.* **101:** 1394–1400.

23. Brooks, A. I., *et al.* (2002). Functional correction of established central nervous system deficits in an animal model of lysosomal storage disease with feline immunodeficiency virus-based vectors. *Proc. Natl. Acad. Sci. USA* **99:** 6216–6221.
24. Hayakawa, M., *et al.* (2002). Muscle-specific exonic splicing silencer for exon exclusion in human ATP synthase gamma-subunit pre-mRNA. *J. Biol. Chem.* **277:** 6974–6984.
25. Ichida, M., *et al.* (2000). Differential regulation of exonic regulatory elements for muscle-specific alternative splicing during myogenesis and cardiogenesis. *J. Biol. Chem.* **275:** 15992–16001.
26. Wolfe, J. H., and Sands, M. S. (1996). Murine mucopolysaccharidosis type VII: a model system for somatic gene therapy of the central nervous system. In *Gene Transfer into Neurons: Towards Gene Therapy of Neurological Disorders* (P. Lowenstein and L. Enquist, Eds.), Wiley, Essex.
27. Den Tandt, W. R., and Scharpe, S. (1991). Characteristics of hexosaminidase A in homogenates of white blood cells using methylumbelliferyl-*N*-acetyl-β-D-glucosaminide-6-sulphate as substrate. *Clin. Chim. Acta* **199:** 231–236.
28. Willott, J. F., Turner, J. G., Carlson, S., Ding, D., Bross, L. S., and Falls, W. A. (1998). The BALB/c mouse as an animal model for progressive sensorineural hearing loss. *Hear. Res.* **115:** 162–174.

Molecular Biology of the Cell
Vol. 17, 966–976, February 2006

# MAGI-1 Is Required for Rap1 Activation upon Cell–Cell Contact and for Enhancement of Vascular Endothelial Cadherin-mediated Cell Adhesion[D] [V]

**Atsuko Sakurai, Shigetomo Fukuhara, Akiko Yamagishi, Keisuke Sako, Yuji Kamioka, Michitaka Masuda, Yoshikazu Nakaoka, and Naoki Mochizuki**

Department of Structural Analysis, National Cardiovascular Center Research Institute, Suita, Osaka 565-8565, Japan

Submitted July 19, 2005; Revised November 28, 2005; Accepted November 29, 2005
Monitoring Editor: Martin A. Schwartz

**Rap1 is a small GTPase that regulates adherens junction maturation. It remains elusive how Rap1 is activated upon cell–cell contact. We demonstrate for the first time that Rap1 is activated upon homophilic engagement of vascular endothelial cadherin (VE-cadherin) at the cell–cell contacts in living cells and that MAGI-1 is required for VE-cadherin-dependent Rap1 activation. We found that MAGI-1 localized to cell–cell contacts presumably by associating with β-catenin and that MAGI-1 bound to a guanine nucleotide exchange factor for Rap1, PDZ-GEF1. Depletion of MAGI-1 suppressed the cell–cell contact-induced Rap1 activation and the VE-cadherin-mediated cell–cell adhesion after $Ca^{2+}$ switch. In addition, relocation of vinculin from cell–extracellular matrix contacts to cell–cell contacts after the $Ca^{2+}$ switch was inhibited in MAGI-1-depleted cells. Furthermore, inactivation of Rap1 by overexpression of Rap1GAPII impaired the VE-cadherin-dependent cell adhesion. Collectively, MAGI-1 is important for VE-cadherin-dependent Rap1 activation upon cell–cell contact. In addition, once activated, Rap1 upon cell–cell contacts positively regulate the adherens junction formation by relocating vinculin that supports VE-cadherin-based cell adhesion.**

## INTRODUCTION

Intercellular adhesion of vascular endothelial cells is essential for connecting neighboring endothelial cells to develop a vascular tree and to function as a barrier separating blood and tissues. Vascular endothelial cell adhesion is characterized by the overlapping of adherens junctions (AJs) and tight junctions (TJs). AJs are constituted by vascular endothelial cadherin (VE-cadherin) in close cooperation with platelet and endothelial adhesion molecule-1 (PECAM-1) and nectin. VE-cadherin-mediated cell adhesion depends on extracellular $Ca^{2+}$, but not those mediated by PECAM-1 and nectin. TJs are made up of junctional adhesion molecule (JAM) family members, occuludin, claudin-5, and nectin (reviewed in Dejana, 2004).

VE-cadherin has an extracellular domain constituted by five cadherin domains, a transmembrane domain, and a cytoplasmic domain connected to p120 catenin and β-catenin (Iyer *et al.*, 2004). Through β-catenin, VE-cadherin is linked to α-catenin that is associated with the actin cytoskeleton, which results in the maintenance of cell–cell adhesion in conjunction with cytoskeleton (Herren *et al.*, 1998; Navarro *et al.*, 1998; Kobielak and Fuchs, 2004). Tyrosine-phosphorylated VE-cadherin in its cytoplasmic domain provides docking sites for signal-transmitting molecules (Esser *et al.*, 1998; Zanetti *et al.*, 2002; Hudry-Clergeon *et al.*, 2005). Conversely, cytoplasmic domain modified by phosphorylation or associated with signaling molecules triggers the inside-out signal that regulates the VE-cadherin-mediated cell adhesion (Nwariaku *et al.*, 2004). β-catenin binds to other signaling molecules including PI3-K and MAGUK with inverted domain structure-1 (MAGI-1) as well as α-catenin (Kotelevets *et al.*, 2005).

MAGI-1 consists of six PSD95/DiscLarge/ZO-1 (PDZ) domains, a guanylate kinase domain and two WW domains flanked by the first and second PDZ domain (Dobrosotskaya *et al.*, 1997). Because PDZ domains are docking domains for PDZ-binding molecules, MAGI-1 associates with a variety molecules such as NMDA (*N*-methyl-D-aspartate) receptors, PTEN, BAI-1, δ-catenin, mNET1, and β-catenin (Hirao *et al.*, 1998; Ide *et al.*, 1999;Mino *et al.*, 2000; Dobrosotskaya, 2001). These MAGI-1-associating molecules function at cell–cell contacts (Laura *et al.*, 2002). MAGI-1, therefore, functions as a scaffold molecule by localizing to cell–cell contacts. Recently, MAGI-1 is reported to biochemically form a complex with E-cadherin and β-catenin (Kawajiri *et al.*, 2000). How-

This article was published online ahead of print in *MBC in Press* (http://www.molbiolcell.org/cgi/doi/10.1091/mbc.E05–07–0647) on December 7, 2005.

[D] [V] The online version of this article contains supplemental material at *MBC Online* (http://www.molbiolcell.org).

Address correspondence to: Naoki Mochizuki (nmochizu@ri.ncvc.go.jp).

Abbreviations used: AJ, adherens junction; CFP, cyan fluorescent protein; ECM, extracellular matrix; EGFP, enhanced green fluorescent protein; FRET, fluorescence resonance energy transfer; GEF, guanine nucleotide exchange factor; GAP, GTPase activating protein; HAEC, human aortic endothelial cell; HUVEC, human umbilical vascular endothelial cell; JAM, junctional adhesion molecule; MAGI-1, MAGUK with inverted domain structure-1; GFP, green fluorescent protein; PBS, phosphate-buffered saline; PDZ, PSD95/DiscLarge/ZO-1; PECAM-1, platelet and endothelial cell adhesion molecule-1; siRNAs, small interfering RNAs; TJ, tight junction; VE-cadherin, vascular endothelial cadherin; VEC-Fc, recombinant VE-cadherin ectodomain-Fc chimera; YFP, yellow fluorescent protein.

ever, the role of the E-cadherin/β-catenin–MAGI-1 complex in cell–cell junctional formation remains elusive.

Rap1 regulates cell–cell adhesion as well as cell–extracellular matrix (cell-ECM) adhesion (Bos, 2005). We have previously demonstrated that Epac-Rap1 signaling enhances VE-cadherin-dependent cell adhesion, thereby stabilizing vascular endothelial cell junctions (Fukuhara *et al.*, 2005). On cell–cell contact, C3G, a guanine nucleotide exchange factor (GEF) for Rap1, is involved in the signaling mediated by E-cadherin and nectin in epithelial cells (Hogan *et al.*, 2004; Fukuyama *et al.*, 2005). Rap1 cycles between GDP-bound inactive form and GTP-bound active form; Rap1-specific GEFs and GTPase activating proteins (GAPs) activate and inactivate Rap1, respectively. Rap1 GEF family consists of C3G (RAPGEF1), PDZ-GEF1 (RAPGEF2), PDZ-GEF2, CalDAG-GEF1, Epac, and Epac2 (Bos *et al.*, 2001).

We here investigate the involvement of MAGI-1–PDZ-GEF1 in the activation of Rap1 on vascular endothelial cell contact and demonstrate that MAGI-1 recruited to cell–cell junctions by associating β-catenin contributes to cell–cell contact-dependent activation of Rap1. In addition, the MAGI-1-mediated signal evoked upon cell–cell contact augments VE-cadherin-dependent endothelial cell adhesion. Thus, engagement of VE-cadherin activates Rap1 via MAGI-1, resulting in positive regulation of VE-cadherin-mediated cell adhesion.

## MATERIALS AND METHODS

### *Plasmids and Adenovirus*

pRaichu-Rap1, Rap1 activation monitoring-probe based on fluorescence resonance energy transfer (FRET), and Adeno-Raichu-Rap1, an adenovirus expressing Raichu-Rap1 were described previously (Mochizuki *et al.*, 2001). Adenoviruses encoding Rap1GAPII and LacZ were obtained from S. Hattori (The Institute of Medical Science, University of Tokyo) and M. Matsuda (Research Institute for Microbial Disease, Osaka University, Osaka, Japan), respectively. Endothelial cells were infected with adenovirus at the appropriate multiplicity of infection for more than 24 h before imaging. The coding sequences of human MAGI-1b (hereafter MAGI-1) and PDZ-GEF1 were amplified by PCR using human heart cDNA library as a template and resultant DNAs were inserted into p3× FLAG-CMV-10 (Sigma, St. Louis, MO) and pEGFP-C1 (Clontech, Palo Alto, CA). cDNAs encoding truncated MAGI-1 as indicated in Figures 3B and 4A were similarly inserted into pEGFP-C1. pCALwL-FLAG-C3G, a FLAG-tagged mammalian expression vector, was obtained from M. Matsuda (Research Institute for Microbial Disease, Osaka University, Osaka, Japan; Ohba *et al.*, 2001). pIRM21-PDZ5 expressed FLAG-tagged PDZ domain 5 of MAGI-1 and internal ribosomal entry site-driven dsFP593 (Nagashima *et al.*, 2002). HcRed-p120 catenin-expressed HcRed-tagged p120 catenin was described previously (Kogata *et al.*, 2003).

### *Reagents and Antibodies*

Purified human immunoglobulin (Ig) G Fc protein was purchased from ICN Biologicals (Cosa Mesa, CA). Glutathione Sepharose, protein A- and G-Sepharose were purchased from Amersham Biosciences (Piscataway, NJ). The rabbit polyclonal anti-MAGI-1b and anti-PDZ-GEF1 antibodies were developed in our laboratory by immunizing rabbits with recombinant glutathione *S*-transferase (GST)-tagged MAGI-1b (aa 1–140) or PDZ-GEF1 (aa 1–250) coupled with complete Freund's adjuvant, respectively. Anti-green fluorescent protein (GFP) antibody was generated in our laboratory. Other antibodies were purchased as follows: anti-Rap1 from Santa Cruz Biotechnology (Santa Cruz, CA); anti-FLAG (M2) and anti-vinculin from Sigma; anti-VE-cadherin, and anti-β-catenin from BD Bioscience (San Jose, CA); anti-ZO-1 from Zymed (South San Francisco, CA), Alexa 488- or Alexa 546-labeled secondary antibodies from Molecular Probes (Eugene, OR); horseradish peroxidase-coupled goat anti-mouse and anti-rabbit IgG from Amersham Biosciences.

### *Cell Culture and Transfection*

Human umbilical vein endothelial cells (HUVECs) and human arterial endothelial cells (HAECs) were purchased from Kurabo (Kurashiki, Japan). The cells were maintained in HuMedia-EG2 with a growth additive set as described previously (Nagashima *et al.*, 2002). Bovine aortic endothelial cells (BAECs), MDCK and 293T cells were maintained in DMEM (Nissui, Tokyo, Japan) supplemented with 10% fetal bovine serum and antibiotics (100 μg of streptomycin and 100 U of penicillin/ml). Endothelial cells and 293T cells were transfected by LipofectAMINE plus reagent (Invitrogen, Carlsbad, CA) and by the calcium phosphate method, respectively.

### *FRET Imaging and Fluorescence Imaging*

HUVECs cultured on collagen-coated glass-base dishes were infected with Adeno-Raichu-Rap1 or transfected with pRaichu-Rap1. The structure of Raichu-Rap1 and the principle of FRET are illustrated as in Figure 1A. Cells were imaged on an Olympus IX-81 inverted fluorescence microscope (Lake Success, NY) as described previously (Nagashima *et al.*, 2002). Dual images for cyan fluorescent protein (CFP) and yellow fluorescent protein (YFP) were obtained through an XF1071 excitation filter, an XF2034 dichroic filter, and an XF3075 emission filter for CFP and an XF 3079 for YFP (Omega Scientific, Tarzana, CA), respectively. The ratio image of YFP/CFP were created by MetaMorph 5.0 software (Universal Imaging, West Chester, PA) and displayed as an intensity-modulated display image as described previously (Nagashima *et al.*, 2002).

Quantitative FRET analysis at the cell–cell contacts was performed by dividing the intensity of YFP by that of CFP in the area defined by randomly selected 30 cell–cell contact sites. The detail was explained in the figure legend of Supplementary Figure 2. Cells expressing either fluorescence-tagged proteins (GFP, dsFP593, and HcRed) were time-lapse imaged similar to FRET imaging on an IX-81 microscope using appropriate filter sets for GFP and dsFP593.

### *Calcium Switch*

HUVECs serum-starved for 10 h in medium 199 (Invitrogen) containing 1% bovine serum albumin (BSA) were transiently exposed to 4 mM EGTA for 30 min to chelate extracellular calcium and disrupt $Ca^{2+}$-dependent intercellular junctions (Volberg *et al.*, 1986). After washing, the cells were allowed to recover in complete cell calcium-containing culture media for the time indicated in the figure (Figures 1D, 6, and 7).

### *Detection of GTP-bound Rap1*

GTP-bound active Rap1 was detected according to Bos's method (Franke *et al.*, 1997). Briefly, cells starved in medium 199 containing 1% BSA for 10 h were subjected to a calcium switch or stimulated with 10 μg/ml VE-cadherin ectodomain-Fc (VEC-Fc) protein for the time indicated at the top of the figure (Figure 1E). The cells were lysed at 4°C in pulldown lysis buffer (20 mM Tris-HCl [pH 7.5], 100 mM NaCl, 10 mM $MgCl_2$, 1% Triton X-100, 1 mM EGTA, 1 mM dithiothreitol, 1 mM $Na_3VO_4$, 1× protease inhibitor cocktail). Precleared lysates were incubated with GST-Rap1 binding domain of RalGDS precoupled to glutathione-Sepharose beads. Proteins collected on the beads were subjected to SDS-PAGE followed by immunoblotting with anti-Rap1 antibody.

### *Immunocytochemistry and Confocal Imaging*

Cells cultured on glass-bottom dishes were fixed with 2% formaldehyde in phosphate-buffered saline (PBS) for 30 min and permeabilized with 0.1% Triton X-100 for 10 min. Cells were blocked with 3% BSA for 30 min and incubated with anti-MAGI-1b, anti-VE-cadherin, anti-ZO-1, anti-vinculin, or anti-β-catenin antibody for 1 h at room temperature. Immunopositive reaction was visualized with Alexa 488- or Alexa 546-labeled secondary antibodies. Confocal images were obtained by an Olympus BX50WI microscope controlled by Fluoview.

### *Immunoprecipitation Assay*

HUVECs were lysed with lysis buffer (100 mM NaCl, 50 mM Tris-HCl [pH 7.5], 1% Triton X-100, 2 mM $Na_3VO_4$, 1× protease inhibitor cocktail). Precleared cell lysates by centrifugation at 15,000 × *g* were incubated with antibodies. Immunoprecipitates collected on protein A- or G-Sepharose were subjected to SDS-PAGE and immunoblotting with antibodies as indicated in the figure (Figures 2D, 3, C, D, and E, and 4C).

### *siRNA-mediated Protein Knockdown*

Small interfering RNAs (siRNAs) targeted to human MAGI-1; 5′-GGACCCUUCUCAGAAGUUCCCUCAA-3′ and 5′-UUGAGGGAACUUCUGAGAAGGGUCC-3, corresponding to nt 843–867 of coding sequence of MAGI-1 cDNA, and that for PDZ-GEF1; 5′-GGGAGUAAUCAAACAAAGAAGACUU3′ and 5′-AAGUCUUCUUUGUUUGAUUACUCCC3′, corresponding to nt 1980–2004 of PDZ-GEF1, were obtained from Invitrogen. VE-cadherin siRNAs were purchased from Santa Cruz Biotechnology. As a control, siRNA duplex with an irrelevant sequence was used. HUVECs were transfected with 20 nM siRNA duplexes using LipofectAMINE 2000 (Invitrogen) according to the manufacturer's instructions and incubated for 48 h after replacing fresh HuMedia-EG2.

### *Cell Adhesion Assay*

Recombinant VEC-Fc chimeric protein was prepared as described previously (Fukuhara *et al.*, 2005). Twenty-four-well tissue culture plates were coated

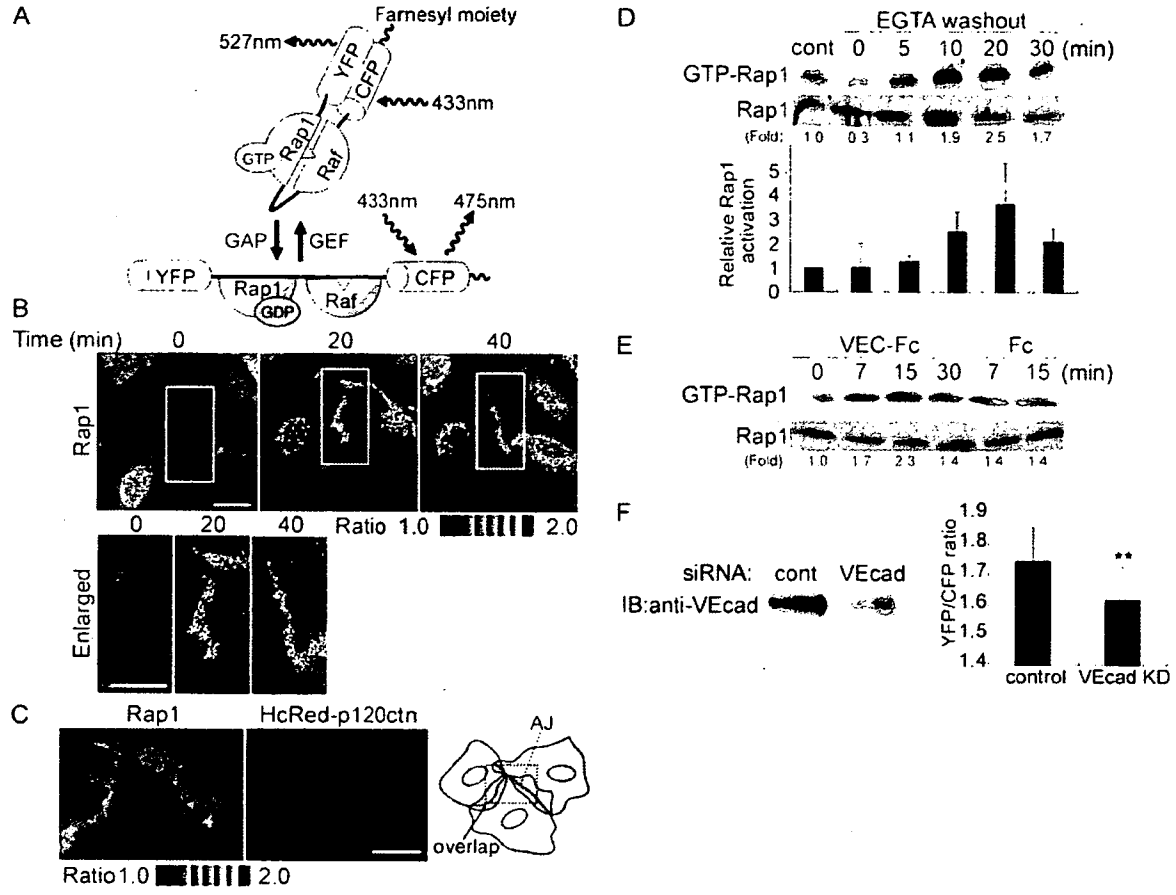


**Figure 1.** Rap1 is activated by VE-cadherin-mediated cell adhesion upon cell–cell contact. (A) Schematic illustration of Raichu-Rap1. FRET efficiency depends on the guanine nucleotide binding state of Rap1. GDP-bound Raichu-Rap1 emits 475-nm fluorescence when excited at 433 nm, whereas GTP-bound Raichu-Rap1 emits 527-nm fluorescence due to FRET. *Raf*; Ras/Rap1 binding domain of Raf. (B) Motile HUVECs infected with Adeno-Raichu-Rap1 were monitored by FRET time-lapse imaging every 20 s. A ratio image of YFP to CFP reflects FRET efficiency. Ratio images are shown by the intensity modulated display, in which the upper and lower limits of the ratio (the intensity of YFP divided by that of CFP) are indicated by the red and blue hues, respectively, and the average intensity of YFP and CFP is used. Time since starting FRET imaging is indicated on the top (min). The boxed regions in the top panels were enlarged and are shown in the bottom panels. Bars, 20 $\mu$m. (C) HUVECs expressing both Raichu-Rap1 and HcRed-tagged p120 catenin were FRET-imaged and red-fluorescence-imaged. The real images of boxed region of the schema are shown as FRET image (left panel) and red-fluorescence image (center). Areas indicated by the gray are regions where protruding and overlapping regions of the contacting cells. Note that Rap1 is activated at the adherens junctions where p120 catenin localizes. Bar, 20 $\mu$m. (D) Confluent HUVECs cultured in medium 199 containing 1% BSA without serum were treated with EGTA for 30 min to disrupt $Ca^{2+}$-dependent cell adhesion. Subsequently, the cells were treated with $Ca^{2+}$-containing medium. Cell lysates at the time points indicated at the top were subjected to pulldown assay for detecting GTP-bound Rap1 as described in *Materials and Methods*. A representative results from three independent experiments is shown (top). Fold activation indicates the ratio of the GTP-Rap1 intensity of total Rap1 intensity to the control GTP-Rap1 intensity of total Rap1 intensity. The result from three independent experiments were shown (bottom). Control (cont) was prepared from cells in medium 199 before calcium switch. Cells treated with EGTA for 30 min (time 0). (E) HUVECs sparsely cultured on the dish were stimulated with 10 $\mu$g/ml VEC-Fc or Fc for the time indicated at the top. Rap1 activity was examined as described for D. Fold activation is analyzed similarly to D. (F) The effect of VE-cadherin siRNA on VE-cadherin expression was examined by immunoblotting (left). FRET at the cell–cell contacts were quantitatively analyzed in control siRNA-treated HUVECs and VE-cadherin-depleted HUVECs (right), as explained in Supplementary Figure 2. Mean values with SDs obtained by 30 cell–cell contact sites are shown as a representative result of three independent experiments. Statistical significance was analyzed by Student's *t* test; ** $p < 0.01$.

with 10 $\mu$g VEC-Fc or Fc protein/ml in PBS-$Ca^{2+}$/$Mg^{2+}$ overnight at 4°C followed by blocking with 1% heat-inactivated BSA in PBS (inactivated at 85°C for 12 min) for 1 h at room temperature. HUVECs treated with control siRNAs or MAGI-1 siRNAs were cultured for 48 h and then suspended in 0.5% BSA-containing Medium 199. Resuspended cells, $2.0 \times 10^5$, were plated and adhered onto each VEC-Fc- or Fc-coated well at 37°C for the indicated time. To analyze cell adhesion to a collagen-covered surface, a collagen-coated 24-well plate (Asahi Technoglass, Chiba, Japan) was used instead of the VEC-Fc-coated plate. After washing with PBS-$Ca^{2+}$/$Mg^{2+}$ four times to remove nonadherent cells, adherent cells and input cells were quantified by measuring endogenous alkaline phosphatase (ALP) activity by using Atto-Phos AP fluorescent substrate system (Promega, Madison, WI).

## RESULTS

### *Rap1 Is Activated on Homophilic VE-Cadherin Association at Cell–Cell Contacts*

Rap1 is previously reported to localize to cell–cell contacts in vascular endothelial cells as well as epithelial cells to stabilize cell–cell contacts (Mandell *et al.*, 2005; Wittchen *et al.*, 2005). However, it remains elusive where Rap1 is activated on cell contacts. To monitor the spatiotemporal activation of Rap1 on vascular endothelial cell–cell contact,

HUVECs expressing Raichu-Rap1 were time-lapse FRET-imaged. Raichu-Rap1 consists of YFP, Rap1, the Ras-binding domain of Raf, CFP, and a CAAX box of Ki-Ras. The intramolecular binding of GTP-Rap1 to Raf induces FRET from CFP to YFP (Figure 1A), whereas the dissociation of Rap1 from Raf reduces FRET. Increased FRET indicated by a red hue was observed at cell–cell contacts during spontaneous movement (Figure 1B and Supplementary Movie 1). Rap1 was constantly activated in the perinuclear region of the cells irrespective of cell–cell contact.

In vascular endothelial cells, the peripheral membrane of cells contacting each other was overlapped. Thus, AJs and TJs are intermingled (Dejana, 2004). To ascertain Rap1 activation at the adherens junctions, HUVECs expressing both Raichu-Rap1 and HcRed-tagged p120 catenin were imaged (Figure 1C). Most of Rap1 activation as indicated by red hue was observed at AJs where p120 catenin was localized. No remarkable Rap1 activation was detected within the protruding membrane overlapping region.

We further quantitatively examined whether the Rap1 is activated during cell adhesion after de-adhesion by chelating extracellular calcium and restoring calcium (hereafter, calcium switch). GTP-bound Rap1 was rapidly increased within 5 min and to a greater extent than the predisruption level by restoration of $Ca^{2+}$ (Figure 1D, top panel). The quantitative results obtained from three independent experiments were shown (Figure 1D, bottom panel). These results suggest that the cell–cell contact triggers the Rap1 activation in a manner dependent on extracellular $Ca^{2+}$. Although Rap1 is reported to be activated in a manner dependent on nectin, which is independent of extracellular $Ca^{2+}$ (Fukuyama *et al.*, 2005), we assumed that $Ca^{2+}$-dependent cell–cell contact triggers Rap1 activation besides nectin-triggered Rap1 activation. We, therefore, examined the VE-cadherin engagement-dependent Rap1 activation. To mimic the VE-cadherin engagement in nascent cell–cell contacts, we used VEC-Fc chimeric protein, which consisted of the extracellular domain of VE-cadherin fused to the Fc portion of Ig. GTP-bound Rap1 was increased when cells were treated with VEC-Fc, but not with control Fc (Figure 1E).

To examine the requirement of VE-cadherin for Rap1 activation upon cell–cell contact, we imaged Rap1 activation in VE-cadherin-depleted HUVECs. Quantitative FRET imaging analysis upon cell–cell contacts demonstrated that Rap1 activation at the cell–cell contacts was less in VE-cadherin-depleted cells than those observed in control siRNA-treated cells (Figure 1F). Collectively, these data indicate that the engagement of VE-cadherin induces Rap1 activation.

### *MAGI-1 Localizes to Cell–Cell Contacts and Binds to β-Catenin*

MAGI-1 constitutes a complex with E-cadherin/β-catenin and associates with a GEF for Rap1, PDZ-GEF1 (Kawajiri *et al.*, 2000), implying that MAGI-1 may link the cadherin-mediated signal to PDZ-GEF1 for the activation of Rap1. To investigate the involvement of MAGI-1 in Rap1 activation on VE-cadherin-mediated cell–cell contact, we first developed an anti-MAGI-1 antibody and examined the expression of MAGI-1 in vascular endothelial cells. MAGI-1 was expressed in all cultured vascular endothelial cells we tested, because it was found in MDCK epithelial cells used as a positive control (Figure 2A). Next, we examined the localization of MAGI-1 in vascular endothelial cells by immunostaining. MAGI-1 was localized to the cell–cell contacts (Figure 2B) and colocalized with VE-cadherin (Figure 2C). The immunopositive reaction in the nucleus appeared to be non-

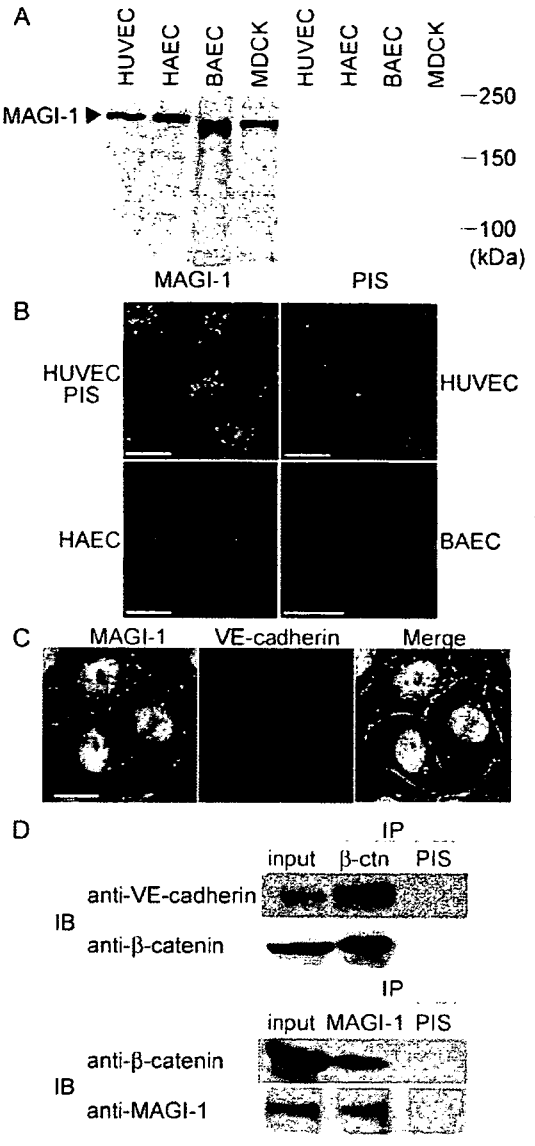


**Figure 2.** MAGI-1 localizes to cell–cell contacts and forms a complex with VE-cadherin and β-catenin. (A) Lysates from the cells indicated at the top were subjected to SDS-PAGE followed by immunoblotting with anti-MAGI-1 antibody (left) and with pre-immune serum (PIS, right). (B) Endothelial cells were immunostained with pre-immune serum (PIS, left top) and anti-MAGI-1 antibody. Immunoreaction was visualized by fluorescent microscopy. Bars, 20 μm. (C) HUVECs were immunostained with both anti-MAGI-1 antibody (green) and anti-VE-cadherin antibody (red). A merged image is shown in the right panel (Merge). Bar, 20 μm. (D) Cell lysates from HUVECs were subjected to either immunoprecipitation (IP) with antibodies as indicated at the top followed by immunoblotting (IB) with antibodies as indicated at the left. VE-cadherin was coimmunoprecipitated with β-catenin (top). β-catenin was coimmunoprecipitated with MAGI-1 (bottom)

specific, because it was detected in the nucleus by immunostaining using preabsorbed anti-MAGI-1 (unpublished data) and after knockdown of MAGI-1 (see Figure 5B).

To investigate how MAGI-1 localizes to cell–cell contacts, we tested the link between VE-cadherin and MAGI-1 by β-catenin. We examined this link by immunoprecipitation

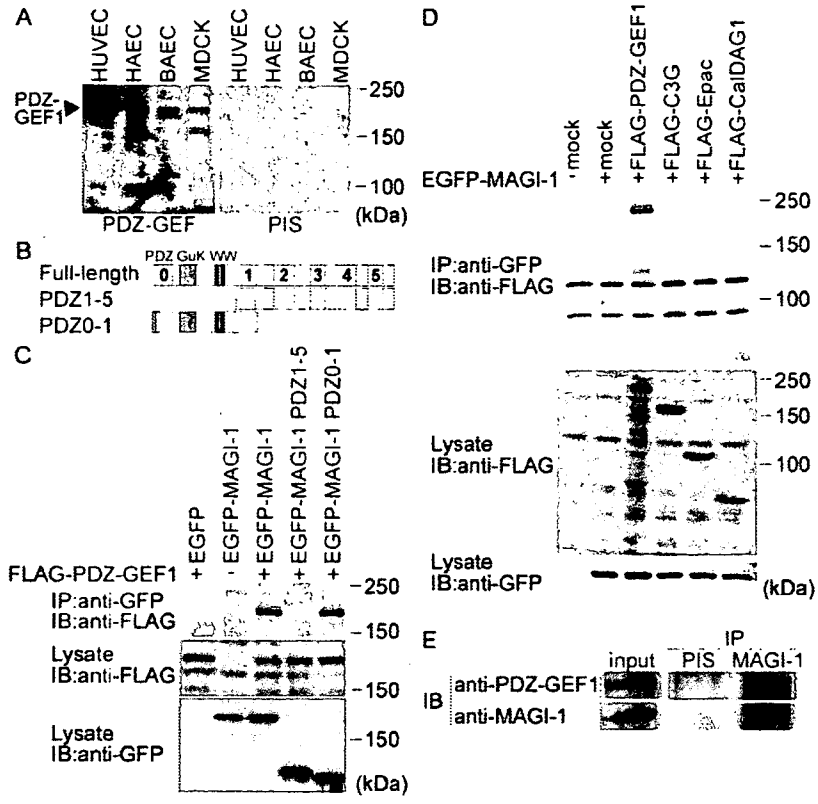


**Figure 3.** MAGI-1 interacts with PDZ-GEF1 in vascular endothelial cells. (A) Cell lysates from HUVECs, HAECs, BAECs, and MDCK cells were subjected to SDS-PAGE and immunoblotting with anti-PDZ-GEF1 antibody (left) or pre-immune serum (PIS, right). (B) Schematic illustration of MAGI-1 (full length) and its deletion mutants. MAGI-1 consists of six PDZ domains (PDZ0–5, indicated by gray boxes), a guanylate kinase domain (GuK), and two WW domains. Deletion mutants, PDZ1–5 and PDZ0–1, consist of PDZ1 to PDZ5 and the amino-terminus to PDZ1, respectively. (C) 293T cells were transfected with the plasmids together with (+) or without (−) FLAG-tagged PDZ-GEF1 expressing vector as indicated at the top. Cell lysates were subjected to immunoprecipitation (IP) with anti-GFP antibody followed by immunoblotting (IB) or directly to immunoblotting using the antibodies as indicated. Note that FLAG-tagged PDZ-GEF1 is coimmunoprecipitated with GFP-tagged PDZ0–1. (D) Cells transfected with a panel of FALG-tagged Rap1 GEF-expressing plasmids together with (+) or without (−) EGFP-tagged MAGI-1-expressing plasmid. Cell lysates were subjected to immunoprecipitation (IP) followed by immunoblotting (IB) similarly to C. Note that only FLAG-tagged PDZ-GEF-1 among several Rap1 GEFs is coimmunoprecipitated with MAGI-1. (E) The lysate of HUVECs was incubated with either pre-immune serum (PIS) or anti-MAGI-1 antibody, followed by immunoblotting with anti-PDZ-GEF1 antibody. Note that MAGI-1 is co-immunoprecipitated with PDZ-GEF1.

assay (Figure 2D). β-catenin bound to both VE-cadherin (Figure 2D, top panel) and MAGI-1 (Figure 2D, bottom panel). These results indicate that MAGI-1 appears to localize to VE-cadherin-based cell adhesion through β-catenin in vascular endothelial cells.

### *MAGI-1 Interacts with PDZ-GEF1 in Vascular Endothelial Cells*

It has been shown that MAGI-1 binds to PDZ-GEF1 localized to cell–cell contacts in epithelial cells (Dobrosotskaya and James, 2000; Kawajiri *et al.*, 2000). We hypothesized that PDZ-GEF1 is associated with MAGI-1 in vascular endothelial cells and that it is involved in the activation of Rap1 on VE-cadherin-mediated cell–cell contact. PDZ-GEF1 was expressed in vascular endothelial cells similarly to MAGI-1 (Figure 3A). The interaction between MAGI-1 and PDZ-GEF1 was examined by the immunoprecipitation using the full-length and the truncated mutants of MAGI-1 (Figure 3, B and C). The PDZ-GEF1 bound to the N-terminus of MAGI-1 (Figure 3C). EGFP-tagged MAGI-1 coimmunoprecipitated PDZ-GEF1, but not other GEFs for Rap1, C3G, Epac1, and CalDAG-GEF-I (Figure 3D). We further examined the interaction between endogenous MAGI-1 and PDZ-GEF1 in HUVECs. Both MAGI-1 and PDZ-GEF1 were coimmunoprecipitated from the lysate of HUVECs (Figure 3E), indicating that PDZ-GEF1 associates with MAGI-1 in vascular endothelial cells.

### *Localization of MAGI-1 to Cell–Cell Contact is Important for Rap1 Activation on Cell Contact*

To understand the role of MAGI-1 in activating Rap1 when forming cell–cell contacts, we proceeded to investigate the localization of MAGI-1 using EGFP-tagged MAGI-1 in motile endothelial cells. EGFP-MAGI-1 was accumulated at cell–cell contacts (Figure 4B, left panels, and Supplementary Movie 2). Removal of the carboxy terminal PDZ domain (delta PDZ5) resulted in the dissociation of MAGI-1 from cell–cell contacts (Figure 4B, right panels, and Supplementary Movie 3). Because it was reported that MAGI-1 binds to β-catenin through PDZ5 (Dobrosotskaya and James, 2000), we tested the requirement of PDZ5 for the association of MAGI1- with β-catenin. β-catenin was coimmunoprecipitated with EGFP-tagged full-length MAGI-1 but not with MAGI-1 lacking PDZ5 (Figure 4C). These results suggest that MAGI-1 localizes to vascular endothelial cell–cell contacts in a manner dependent on β-catenin. We further revealed that MAGI-1 was dislocated from the cell–cell contact of the PDZ5-expressing cells as marked by red fluorescence but not from that of wild-type cells (Figure 4D), indicating that PDZ5 is important for the localization of MAGI-1 to cell–cell contacts.

To examine the requirement of the association of MAGI-1 with β-catenin for the cell–cell contact-induced Rap1 activation, we checked the effect of disconnection of MAGI-1 to β-catenin by overexpressing MAGI-1 PDZ domain 5 on Rap1 activation. In HUVECs expressing MAGI-1 PDZ domain 5, as marked by dsFP593 (Figure 4E and Supplementary Movie 4), Rap1 activation upon cell–cell contacts was not observed in FRET imaging. These results indicate that the dislocation of MAGI-1 from the cell–cell contact inhibits Rap1 activation at the cell–cell contacts in motile vascular endothelial cells.

To confirm the requirement of MAGI-1 in Rap1 activation upon vascular endothelial cell–cell contact, we knocked down MAGI-1 in HUVECs using RNA interference. MAGI-1